Structural Properties of Micelles formed by Telechelic Pentablock Quaterpolymers with pH-responsive Midblocks and Thermo-responsive End Blocks in Aqueous Solution

Florian A. Jung,[†] Panayiota A. Panteli,[‡] Chia-Hsin Ko,[†] Jia-Jhen Kang,[†] Lester C. Barnsley,[§] Constantinos Tsitsilianis,[∥] Costas S. Patrickios,[‡] Christine M. Papadakis[*,†]

[†] Fachgebiet Physik weicher Materie, Physik-Department, Technische Universität München, James-Franck Str. 1, 85748 Garching, Germany

[‡]Department of Chemistry, University of Cyprus, P.O. Box 20537, 1678 Nicosia, Cyprus

[§] Jülich Centre for Neutron Science (JCNS) at Heinz Maier-Leibnitz Zentrum (MLZ), Forschungszentrum Jülich GmbH, Lichtenbergstr. 1, 85748 Garching, Germany

[∥]Department of Chemical Engineering, University of Patras, 26504 Patras, Greece

KEYWORDS. Amphiphilic polymers, multi-responsive polymers, solution behavior, dynamic light scattering, small-angle neutron scattering, small-angle X-ray scattering

TABLE OF CONTENTS GRAPHIC

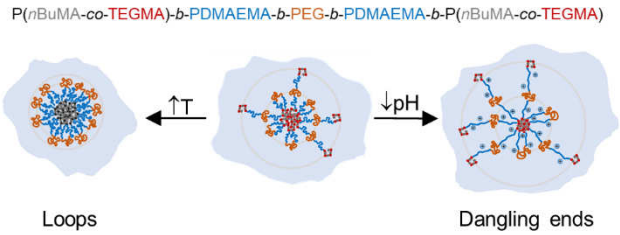

ABSTRACT

We investigated the structural properties of dynamic micelles arising from the self-assembly of the multi-responsive pentablock quaterpolymer P(*n*BuMA$_8$-*co*-TEGMA$_8$)-*b*-PDMAEMA$_{50}$-*b*-PEG$_{46}$-*b*-PDMAEMA$_{50}$-*b*-P(*n*BuMA$_8$-*co*-TEGMA$_8$) (*n*BuMA, TEGMA, DMAEMA and EG are *n*-butyl methacrylate, tri(ethylene glycol) methyl ether methacrylate, 2-(dimethylamino)ethyl methacrylate and ethylene glycol, respectively) in aqueous solution using a combination of scattering methods. In this multisegmented polymer, a pH-responsive BAB triblock copolymer from the weak cationic polyelectrolyte PDMAEMA and the hydrophilic PEG is end-capped by two blocks comprising random sequences of thermo-responsive TEGMA units and hydrophobic *n*BuMA units. Dynamic light scattering (DLS) revealed the existence of single micelles and small clusters in dilute aqueous solution. The hydrodynamic radius of the micelles depends strongly on pH and temperature. The inner structure of the micelles was investigated by small-angle X-ray scattering and small-angle neutron scattering (SAXS and SANS) and static light scattering (SLS), and micelles with a hydrophobic core containing a rather high fraction of water and a strongly swollen corona were found. The ratio of loops and dangling ends depends on temperature and pH.

INTRODUCTION

Amphiphilic block copolymers have interesting properties due to their tendency to self-assemble in selective solvents.[1] Diblock copolymers with one hydrophilic block and one hydrophobic block have been studied extensively and have been shown to form micelles in aqueous solution.[2–6] Among many other potential applications, they have been used as drug delivery systems and nanomedicine applications.[7,8] Block copolymers with three or more blocks allow access to even more morphologies and functionalities.[9] In the case of triblock copolymers with hydrophilic blocks A and hydrophobic blocks B, micelles may be star-like (ABA) or flower-like (BAB).[10,11] A prominent example for the former are the Pluronics® which have been widely studied and have been used in medical applications.[12] They are also called telechelic block copolymers.

In order for flower-like micelles to form, both end blocks have to be located in the same micellar core. To achieve this, the hydrophilic midblock has to form a loop, which imposes an entropic penalty on the free energy.[10] The magnitude of this penalty depends on the length of the midblock and its rigidity. If the entropic penalty is larger than the free energy gained by associating both end blocks into the hydrophobic core of the micelle, e.g. if the hydrophobicity of the end blocks is low, one end block will instead extend into the surrounding water and form a so-called dangling end.[13,14] At high concentrations, intermicellar bridges may form, i.e., two micelles are connected by incorporating one end block into the micellar core of an adjacent micelle.[15] This way, loose clusters of a number of bridged micelles or, at concentrations larger than the critical gel concentration, *cgc* (percolation threshold), a transient network, or hydrogel, are formed.[16] Since the crosslinks are based on hydrophobic association of the end blocks, they are physical and non-covalent, which results in unique mechanical properties of the hydrogel, such as a high toughness.[17] Furthermore,

the hydrogels are able to self-heal due to the fully reversible nature of the hydrophobic crosslinks, making them especially interesting for tissue engineering applications.[18]

Smart hydrogels are based on stimuli-responsive block copolymers.[19] Many studies have addressed responsive triblock copolymers[20–22] and have recently extended to block copolymers with more than three blocks[23], e.g. pentablock copolymers.[24–29] pH and temperature are among the most studied stimuli due to their relevance for biomedical applications.

Weak polyelectrolytes are pH responsive polymers which become ionized in a certain pH range. The additional ionic repulsive interactions lead to an extended/stretched conformation of the polyelectrolyte chain. Thus, for hydrogels based on telechelic block copolymers, with a polyelectrolyte midblock adopting a stretched conformation in the ionized state, bridges are favored over loops promoting gel formation already at very low concentrations.[30,31] Furthermore, using pH-responsive polyampholytes as midblocks allow to switch between positively and negatively charged networks.[32,33]

Thermo-responsive polymers undergo a transition from hydrophilic to hydrophobic at a certain temperature.[34] When the transition is triggered by increasing temperature, the behavior is of lower critical solution temperature (LCST) type. LCST-type polymers have been used as midblocks to tune the swelling capability of hydrogels based on telechelic block copolymers,[35,36] or as end blocks to tune the gelation behavior.[37–39] In the latter case, the end blocks are hydrophilic at temperatures below the LCST and do not associate. Increasing the temperature above the LCST induces hydrophobic association of the end blocks and therefore serves as an effective switch between a liquid-like solution and a hydrogel (sol-gel transition).

The transition temperature of the end blocks and thus the sol-gel transition may be modified by using random copolymers as end blocks.[40] While strong hydrophobic interactions between purely

hydrophobic blocks may prevent exchange of end blocks between micellar cores, thus bringing the system into a kinetically frozen state,[41] the random copolymers may exhibit weaker interactions and are therefore more dynamic.[42] Incorporating pH responsive ionic moieties in random copolymer end blocks resulted in higher exchange rates with increasing degree of charge of the polyelectrolyte.[43,44]

Along this line, the incorporation of LCST-type monomers to the associative hydrophobic blocks allows to control their exchange dynamics via temperature variation. This concept was recently exemplified by designing a telechelic triblock terpolymer having a hydrophilic (and pH-responsive) poly(2-(dimethylamino)ethyl methacrylate) (PDMAEMA) midblock and random copolymer end blocks, comprising hydrophobic *n*-butyl methacrylate (*n*BuMA) monomers and thermo-responsive (LCST-type) triethylene glycol methyl ether methacrylate (TEGMA) monomers.[45] Rheological studies on solutions with concentrations above the *cgc* and neutral pH revealed a strong dependence of the mechanical properties of the hydrogel on temperature. At low temperatures, the system behaves like a dynamic network, while at high temperatures, the network is frozen, as seen from the increase of viscosity by a few orders of magnitude upon raising the temperature from 5 °C to 45 °C. It is also worth noting that, even at the lowest temperatures, where PTEGMA is water-soluble, a network is formed, owing to the dominant, permanently hydrophobic *n*BuMA monomers. Structural investigations with small-angle neutron scattering (SANS) showed that the aggregation number of the micelles increases with temperature and that the micellar cores contain a significant amount of water, which varies with temperature.

Instead of symmetric random-block terpolymers of (A-*co*-B)-*b*-C-*b*-(A-*co*-B) type, another macromolecular topology was recently used to control the dynamic character of association, namely block-gradient copolymers of (A-*grad*-B)-*b*-A type, comprising an associative

poly(styrene-*grad*-2-dimethylamino acrylate) block, covalently bound to poly(dimethylamino acrylate). This kind of asymmetric[46] block copolymers self-assemble reversibly into micelles in aqueous solutions, triggered by both pH and temperature.[47]

In the present work, we investigate a telechelic pentablock quaterpolymer with symmetric (C-*co*-D)-*b*-B-*b*-A-*b*-B-*b*-(C-*co*-D) topology in aqueous solution. The end blocks are statistical copolymers from TEGMA and *n*BuMA units. The middle part BAB consists of two dual responsive B blocks from PDMAEMA and a hydrophilic A block from poly(ethylene glycol) (PEG). PTEGMA is a thermoresponsive polymer with LCST behavior in aqueous solution, i.e., it is water-soluble below its cloud point of ~52 °C and water insoluble above,[48] while P*n*BuMA is permanently hydrophobic. Thus, P(TEGMA-*co*-*n*BuMA) random copolymers are expected to have a composition-dependent LCST. PDMAEMA is a weak cationic polyelectrolyte and therefore pH-responsive. At pH values below its pK_a of ~7, the tertiary amine groups are ionized and become positively charged. Furthermore, in its nonionized state, PDMAEMA is thermoresponsive and has a pH-dependent LCST.[49,50] PEG is hydrophilic (with very high LCST) and provides stealth properties to the micellar self-assemblies.

Thus, the polymer architecture is similar to the one of the previously investigated telechelic triblock terpolymer described above.[45] The middle part of the present pentablock quaterpolymer has altogether the same length as the PDMAEMA midblock in the previously investigated triblock terpolymer, but now features a PEG block which is expected to guarantee water solubility of the middle part (and thus gel formation) even when the PDMAEMA blocks are in the poor solubility state, e.g. at high pH and high temperatures. Moreover, the end blocks are shorter than in the previously studied polymer, and the *n*BuMA content is slightly lower, resulting in enhanced dynamic exchange (dynamic stickers) and a slightly higher transition temperature. We focus on

the structural properties of the micelles formed by this polymer, i.e., at concentrations below the percolation threshold, *cgc*, and on the effect of pH on their thermo-responsive behavior. At this, we use a combination of scattering methods, targeting different length scales.

The manuscript is structured as follows: After the Experimental Section, results of a dynamic light scattering (DLS) study on dilute solutions in dependence on pH and temperature values are presented. Afterwards, a detailed SANS investigation is outlined and corroborated by results from small-angle X-ray scattering (SAXS) and static light scattering (SLS) measurements. Finally, the results are summarized.

EXPERIMENTAL SECTION

Materials

Most chemicals were purchased from Sigma-Aldrich-Merck and used as received unless otherwise noted: 4,4′-azobis(4-cyanovaleric acid) (ACVA, ≥98%), 2-azobisisobutyronitrile (AIBN, 98%), *n*-butyl methacrylate (*n*BuMA, 99%), calcium hydride (CaH_2, 90-95%), carbon disulfide (CS_2, ≥99%), deuterated chloroform ($CDCl_3$, 99.8 atom%), dichloromethane (DCM, >99%), diethyl ether (>99%), 2-(dimethylamino)ethyl methacrylate (DMAEMA, 98%), N,N′-dicyclohexylcarbodiimide (DCC, ≥99%), 4-dimethylaminopyridine (DMAP, 99%), 1,4-dioxane (≥99%), 1-dodecanethiol (≥98%), ethanol (EtOH, 96%), ethyl acetate (EtOAc, >99.8%), *n*-hexane (≥95%), iodine (I_2, ≥99%), methanol (MeOH, ≥99.8%), poly(ethylene glycol) (PEG-diol, Mw = 2050 g mol–1), sodium hydride (NaH, 60% dispersion in mineral oil), sodium thiosulfate pentahydrate ($Na_2S_2O_3{\cdot}5H_2O$), and tri(ethylene glycol) methyl ether methacrylate (TEGMA, 93%). Tetrahydrofuran (THF) and magnesium sulfate anhydrous ($MgSO_4$, 98%) were purchased from Scharlau, Spain. DMAEMA, *n*BuMA, and 1,4-dioxane were stirred over calcium hydride for at least 3 days and vacuum-distilled just prior to use, while TEGMA was passed through a basic

alumina (Al_2O_3) column to remove the polymerization inhibitor. AIBN was purified after recrystallization from ethanol. The synthesis of the 4-cyano-4-(((dodecylthio)carbonothioyl)thio)pentanoic acid (CDCTPA) RAFT agent was accomplished according to the literature.[51]

Polymer Synthesis

Synthesis of the PEG difunctional macroRAFT agent.

Synthesis of the difunctional RAFT chain transfer agent was accomplished through the bisesterification reaction of 4-cyano-4-(((dodecylthio)carbonothioyl)thio)pentanoic acid (CDCTPA) and PEG in the presence of DCC activator and DMAP catalyst. To this end, 2.4 g of CDCTPA (5.95 mmol, 2.44 eq. relative to PEG), and 0.073 g of DMAP (0.595 mmol, 0.1 equivalent) were transferred in a round-bottomed flask and dissolved in 12.3 mL of DCM (20% w/v). In another flask, 5.0 g of PEG-diol (2.44 mmol, 1 eq.) were dissolved in 25 mL of DCM (20% w/v), and the resulting solution was added into the round-bottomed flask containing CDCTPA and DMAP. In a third flask, 1.35 g of DCC (6.54 mmol, 1.1 eq.) was dissolved in 6.7 mL DCM (20% w/v), and the resulting solution was subsequently added dropwise to the solution containing PEG, CDCTPA, and DMAP. The reaction was left under stirring for 20 h at room temperature. Then, the produced urea compound was removed by filtration, and the desired PEG macroRAFT CTA was purified via column chromatography using a mixture of DCM and MeOH at a volume ratio of 95:5. Finally, after its complete drying in a vacuum oven for 24 h, the PEG macroRAFT CTA was stored in the refrigerator.

Synthesis of the pentablock quaterpolymer using RAFT polymerization.

The synthesis of the (nBuMA$_8$-*co*-TEGMA$_8$)-*b*-DMAEMA$_{50}$-*b*-EG$_{46}$-*b*-DMAEMA$_{50}$-*b*-(nBuMA$_8$-*co*-TEGMA$_8$) pentablock quaterpolymer was accomplished in two steps using

sequential RAFT polymerization. To this end, a solution of 1 g of DMAEMA (6.36 mmol, 100 eq.), 0.181 g of the PEG difunctional macroRAFT CTA agent (6.36 × 10−5 mol, 1 eq.), 6.5 mg of AIBN (3.98 × 10−5 mol, 0.625 eq.), in 2.3 g of 1,4-dioxane was transferred to a 15 mL Schlenk flask equipped with a magnetic stirring bar. The solution was degassed by three freeze-pump-thaw cycles, and the Schlenk flask containing it was subsequently placed in an oil bath thermostated at 65 °C for 20 h, after which period the DMAEMA monomer conversion to polymer reached 99%. Then, a solution of 0.181 g of *n*BuMA (1.27 mmol, 20 eq.), 0.295 g of TEGMA (1.27 mmol, 20 eq.), in 1 g of 1,4-dioxane was transferred to a 10 mL Schlenk flask equipped with a magnetic stirring bar. After being degassed by three freeze-pump-thaw cycles, the solution was added into the Schlenk flask containing the 1,4-dioxane solution of $DMAEMA_{50}$-*b*-EG_{46}-*b*-$DMAEMA_{50}$ triblock copolymer just prepared. The polymerization of the *n*BuMA and TEGMA monomers was left to proceed for 18 h, after which period their conversions to polymer reached 80%. The produced (nBuMA$_8$-*co*-TEGMA$_8$)-*b*-$DMAEMA_{50}$-*b*-EG_{46}-*b*-$DMAEMA_{50}$-*b*-(nBuMA$_8$-*co*-TEGMA$_8$) pentablock quaterpolymer was obtained by precipitation in *n*-hexane and drying in a vacuum oven for 24 h.

Molecular Characterization

Gel Permeation Chromatography (GPC).

The triblock copolymer precursor and the final pentablock quaterpolymer were characterized in terms of their molecular weights and molecular weight distributions using GPC. A single PL Mixed "D" column, packed with polymer beads of 5 μm diameter and pore sizes of 100, 500, 10^3 and 10^4 Å, purchased from Polymer Laboratories, was used. THF served as the mobile phase, and it was delivered at a flow rate of 1 mL min^{-1} using a Waters 515 isocratic pump. An ERC-7515A refractive index (RI) detector, also from Polymer Laboratories, was used for the measurement of

the RI signal. The calibration curve was performed using ten linear poly(methyl methacrylate) (polyMMA) standards having molecular weights equal to 0.8, 2.2, 6.4, 12.6, 23.5, 41.4, 84.3, 201, 342, and 675 kg mol^{-1} and narrow molecular weight distributions, purchased from Polymer Standards Service (PSS) GmbH in Germany.

Nuclear Magnetic Resonance (NMR) Spectroscopy.

The ^1H NMR spectra were recorded in $CDCl_3$ using a 500 MHz Avance spectrometer equipped with an Ultrashield magnet purchased from Bruker, Massachusetts, USA. The produced triblock copolymer precursor and the final pentablock quaterpolymer were characterized for the determination of monomer-to-polymer conversion, and comonomer compositions and theoretical molecular weights using ^1H NMR spectroscopy.

Table 1. Molecular weights, molecular weight dispersity, and compositions of the copolymer determined using GPC (Figure S1 in the Supporting Information) and ^{1}H NMR spectroscopy (Figure S2 in the Supporting Information).

	Polymer Structure	Polymerization Time (h)	Monomer conversion (%)	Theoretical MW	GPC			*n*BuMA or TEGMA (mol%)	
					M_p	M_n	$Đ$	Theoretical	^{1}H NMR
1	PDMAEMA$_{50}$-*b*-PEG$_{46}$-*b*-PDMAEMA$_{50}$	20	99	18471	15900	10100	1.60	0.0	0.0
2	P(*n*BuMA$_8$-*co*-TEGMA$_8$)-*b*-PDMAEMA$_{50}$-*b*-PEG$_{46}$-*b*-PDMAEMA$_{50}$-*b*-P(*n*BuMA$_8$-*co*-TEGMA$_8$)	18	80 (*n*BuMA) 80 (TEGMA)	24455	17600	12500	2.07	12.1 12.1	12.8 12.0

Sample Preparation

Aqueous solutions were prepared by dissolving the polymer in D_2O (99.95%, Deutero GmbH) at concentrations of 1 wt% (DLS and SAXS) or 2 wt% (SANS) and by stirring the mixture overnight. Then, the solutions were filtered with a 0.8 μm cellulose mixed ester (CEM) syringe filter, and again stirred overnight. Afterwards, the pH of the solution was adjusted using small amounts of 1 M HCl. By eye, none of the samples were found to form a gel.

The dissociation constant pK_a was determined by adding 1M HCl to a 1 wt% polymer solution in D_2O. The pH value was measured using a Metrohm 826 pH meter with a glass electrode and was converted to pD using the relation pD = pH + 0.4.[52]

Dynamic Light Scattering (DLS) and Static Light Scattering (SLS)

For DLS and SLS measurements, we used a LS Spectrometer (LS Instruments, Fribourg, Switzerland). It was equipped with a polarized HeNe laser (Thorlabs, Dachau, Germany) with a maximum power output of 21 mW and a wavelength of 632.8 nm, a goniometer for multiangle measurements and two avalanche photodiode (APD) detectors. The temperature of the sample was controlled by placing it in a heatable bath of index matching solvent (mixed *trans*- and *cis*-decalin). Sample holders were cylindrical glass cuvettes with outer diameter 5 mm and wall thickness 0.4 mm. Measurements were performed at scattering angles θ between 60° and 120°. For DLS, 10 normalized intensity autocorrelation functions, $g_2(q,\tau)$, were recorded for 30 s at all angles using a multi-tau correlator and were subsequently averaged after removing outliers. $q = 4\pi n/\lambda \times \sin(\theta/2)$ is the momentum transfer, where n is the refractive index of the solvent and λ the wavelength of the laser light. $g_2(q,\tau)$ is related to the normalized electric field autocorrelation function, $g_1(q,\tau)$, by the Siegert relation, $g_2(q,\tau) - 1 = \beta|g_1(q,\tau)|^2$, with the coherence factor β (usually close to 1).

We used two approaches to model the autocorrelation curves: (i) by numerical inverse Laplace transformation calculating the distributing function of hydrodynamic radii, G(R_h), using the software REPES.[53,54] At this, a probability to reject of 0.5 was chosen (unless stated otherwise). The distributions were normalized to the height of the most prominent peak. They are given in the equal area representation $G(R_h)R_h$ vs. log(R_h). (ii) A linear combination of a fast, single exponential decay and a slow, stretched exponential decay was fitted, which describes a bimodal distribution of coexisting single micelles and clusters:

$$g_1(q,\tau) = A_{mic}e^{-\Gamma_{mic}\tau} + (1 - A_{mic})e^{-(\Gamma_{clu}\tau)^{\nu}} \quad (1)$$

A_{mic} is the amplitude of the fast decay and related to the relative amount of single micelles, Γ_{mic} and Γ_{clu} are the respective decay rates and ν the stretching exponent. From the decay rates, diffusion coefficients were calculated by $D_{mic} = \Gamma_{mic}/q^2$ and $D_{clu} = (\Gamma_{clu}\nu)^{-1}\Gamma(\nu^{-1})/q^2$. $\Gamma(x)$ is the gamma function. The hydrodynamic radii were determined using the Stokes-Einstein equation:

$$R_h = \frac{k_B T}{6\pi\eta D} \quad (2)$$

where k_B is Boltzmann's constant, T the temperature and η the viscosity of the solvent.

For SLS, the angle-dependent, average scattering intensity I_{avg} was corrected for the background from D_2O, I_{D2O}, and brought to absolute scale, using the scattering intensity of toluene, I_{tol}, as a reference:

$$I_{SLS}(q) = \frac{I_{avg}(q) - I_{D2O}(q)}{I_{tol}(q)} R_{tol} \quad (3)$$

R_{tol} is the Rayleigh ratio of toluene, which amounts to 1.34×10^{-5} cm^{-1}.[55]

Small-angle Neutron Scattering (SANS)

SANS experiments were conducted at instrument KWS-1 operated by the Jülich Centre for Neutron Science (JCNS) at Heinz-Meier-Leibnitz Zentrum (MLZ) in Garching, Germany.[56,57] The

neutron wavelength was set to λ = 5 Å using a Dornier velocity selector ($\Delta\lambda/\lambda$ = 10 %), and measurements were carried out at sample-to-detector distances of 1.5 m, 8 m and 20 m with durations of 300 s, 1200 s and 1800 s, respectively, which allowed us to cover a large *q*-range from 0.003 to 0.445 $Å^{-1}$. The samples were mounted in quartz cuvettes (Hellma 110-QS) with a path length of 2 mm. Temperatures were controlled using a thermostated sample holder (Peltier) and were varied between 10 °C and 60 °C. Measurements were performed after stabilizing the temperature for at least 5 minutes. The scattered neutrons were recorded using a scintillation detector with 128 × 128 channels. The intensity matrices were corrected for detector efficiency, background noise, sample transmission and scattering from the empty cell. Prior to azimuthal averaging, the solvent (D_2O) contribution was subtracted from the scattering of the samples. At this, the D_2O fraction was approximated by unity. The intensity was brought to absolute scale using plexiglass as a secondary standard. Data reduction was performed using the software QtiKWS provided by JCNS.

Small-angle X-ray Scattering (SAXS)

SAXS investigations were carried out using an S3-Micro Kratky camera (HECUS, Austria). The wavelength was 0.154 nm, and the beam had dimensions of 1 mm × 0.2 mm (H × V). The detector was a PILATUS 100k with a pixel size of 172 μm, mounted at sample-to-detector distance of 291.5 mm. The samples were mounted in cylindrical quartz capillaries with a diameter of 1.5 mm. Temperatures were controlled using a thermostated sample holder (Peltier). After each temperature change, the sample was equilibrated for several minutes before performing a measurement. The intensities were azimuthally averaged, corrected for background from the D_2O filled capillary and the transmissions and were brought to absolute scale using water as a standard.

SANS, SAXS and SLS data analysis

The full scattering curves were modeled following an approach by Lund et al., which describes the scattering from micelles with a spherical core, potentially having a surface roughness, and a swollen shell, which coexist with their clusters:[58,59]

$$I(q) = \frac{\phi}{V_{mic}}[f_{clu}N_{clu}S_{clu}(q) + (1 - f_{clu})]P_{mic}(q) + I_{bg} \quad (4)$$

ϕ is the polymer volume fraction and V_{mic} the micellar volume. For the solutions investigated in the present work, ϕ has values of 0.012 (1 wt%) and 0.023 (2 wt%). f_{clu} is the fraction of clusters, which consist of N_{clu} randomly connected micelles. The correlation of the clusters is described by the structure factor $S_{clu}(q)$. $P_{mic}(q)$ is the form factor of a single micelle. I_{bg} is a constant background.

The cluster structure factor $S_{clu}(q)$ is given by[60]

$$S_{clu}(q) = \frac{2}{1-\sin(qD)/qD} - 1 - \frac{2\left[1-(\sin(qD)/qD)^{N_{clu}}\right]}{N_{clu}(1-\sin(qD)/qD)^2}\frac{\sin(qD)}{qD} \quad (5)$$

with D being the distance between micelles. The micellar form factor has four contributions: the scattering of the core, $A_c(q)$, the scattering of the shell, $A_{sh}(q)$, a cross term between core and shell, and the chain scattering from polymers in the shell, $B(q)$:

$$P_{mic}(q) = {\Delta\rho_c}^2 {N_{agg}}^2 {V_c}^2 A_c(q)^2 + {\Delta\rho_{sh}}^2 N_{agg}\left(N_{agg} - B(0)\right){V_{sh}}^2 A_{sh}(q)^2 +$$

$$2\Delta\rho_c\Delta\rho_{sh}{N_{agg}}^2 V_c V_{sh} A_c(q)A_{sh}(q) + {\Delta\rho_{sh}}^2 N_{agg}{V_{sh}}^2 B(q) \quad (6)$$

N_{agg} is the aggregation number of the micelle. $\Delta\rho_c$ and $\Delta\rho_{sh}$ are the excess scattering length densities (SLD) of core and shell, respectively, with respect to the solvent. In this work, they were calculated to be 0.62×10^{-6} Å^{-2} (core), 0.64×10^{-6} Å^{-2} (shell) and 6.38×10^{-6} Å^{-2} (D_2O) for neutrons and 9.02×10^{-6} Å^{-2} (core), 8.85×10^{-6} Å^{-2} (shell) and 9.43×10^{-6} Å^{-2} (D_2O) for X-rays. (The effect of D_2O in the core and the shell is included as described below.) The mass densities (in g/cm^3) used for calculating the SLDs were 1.11 (D_2O), 0.89 (*n*BuMA), 1.03 (TEGMA), 0.93 (DMAEMA)

and 1.12 (EG). V_c and V_{sh} are the volumes of the core and shell blocks, respectively. For the polymer in this work, they are defined as

$$V_c = (1 + f_{loop})V_B \quad (7)$$

$$V_{sh} = V_{ACA} + (1 - f_{loop})V_B \quad (8)$$

with f_{loop} the fraction of chains forming loops, V_B the volume of the copolymer end block and V_{ACA} the volume of the mid triblock copolymer. The core and shell scattering contributions are given by

$$A_c(q) = \frac{3(\sin(qR_c) - qR_c\cos(qR_c))}{(qR_c)^3} e^{-q^2{\sigma_{int}}^2/2} \quad (9)$$

$$A_{sh}(q) = \frac{1}{C}\int_{R_c}^{\infty} 4\pi r^2 n_{sh}(r)\frac{sin(qr)}{qr}\mathrm{d}r\, e^{-q^2{\sigma_{int}}^2/2} \quad (10)$$

where R_c is the radius of the micellar core, σ_{int} the roughness of the core-shell interface and C a normalization constant given by

$$C = \int_{R_c}^{\infty} n_{sh}(r)4\pi r^2 dr \quad (11)$$

$n_{sh}(r)$ is the density profile of the shell which is chosen as

$$n_{sh}(r) = r^{-x}/\left(1 + \exp\left(\frac{r - R_m}{\sigma_m R_m}\right)\right) \quad (12)$$

R_m is the total radius of the micelle, σ_m the relative width of the micellar surface and x a scaling exponent describing the steepness of the decay. For all model fits in this work, x was fixed at 4/3, which represents a density profile of starlike micelles.[61] Assuming a certain fraction of water, f_{water}, inside the micellar core, R_c can be directly calculated by:

$$R_c = \left(\frac{3N_{agg}V_c}{4\pi(1 - f_{water})}\right)^{1/3} \quad (13)$$

The chain scattering is approximated by

$$B(q) = \frac{P_{chain}(q)}{1 + vP_{chain}(q)} \quad (14)$$

ν is a parameter describing the interaction between the chains in the shell. P_{chain} is the chain form factor, which is approximated by the Beaucage model:[62]

$$P_{chain}(q) = e^{-q^2 {R_{g,shell}}^2/3} + \frac{d_f}{{R_{g,shell}}^{d_f}} \Gamma\left(\frac{d_f}{2}\right) \left(\frac{erf\left(kqR_{g,shell}/\sqrt{6}\right)^3}{q} \right)^{d_f} \quad (15)$$

$R_{g,shell}$ denotes the radius of gyration of the polymer chains in the shell, d_f their fractal dimension and k is a constant set to 1.06.[62] Γ(x) and erf(x) are the gamma function and the error function, respectively.

All fits were performed using self-written procedures in Python and were based on a least-square method. For SANS, smearing effects due to instrumental resolution were included following standard procedures.[63]

RESULTS AND DISCUSSION

To choose relevant pD values for the structural and dynamic studies, the degree of ionization of the PDMAEMA blocks is determined first. Then, the solution behavior of P(*n*BuMA$_8$-*co*-TEGMA$_8$)-*b*-PDMAEMA$_{50}$-*b*-PEG$_{46}$-*b*-PDMAEMA$_{50}$-*b*-P(*n*BuMA$_8$-*co*-TEGMA$_8$) is characterized in temperature scans at several pD values in the range 1.9-8.5, i.e., around the pK_a value of PDMAEMA. Using DLS, micelles and clusters are detected, and the inner structure of the micelles is investigated in detail using SANS. The model used for analyzing the SANS data is verified using a combination of SAXS and SLS.

In Figure 1a, the titration curve, obtained by adding 1 M HCl to a 1 wt% D_2O solution is shown. The curve has the typical shape for a weak base being diluted by a strong acid. From the equivalence point and corresponding half-equivalence point, we determined the dissociation constant, pK_a, to be 7.5. This value is attributed to the PDMAEMA block, and is comparable to values reported in literature.[50,64] The resulting degree of ionization, α, of PDMAEMA as a function

of pD, as calculated from $\alpha = (1 + 10^{pD - pKa})^{-1}$, is shown in Figure 1b. The α values and corresponding pD values investigated in this work are indicated as well.

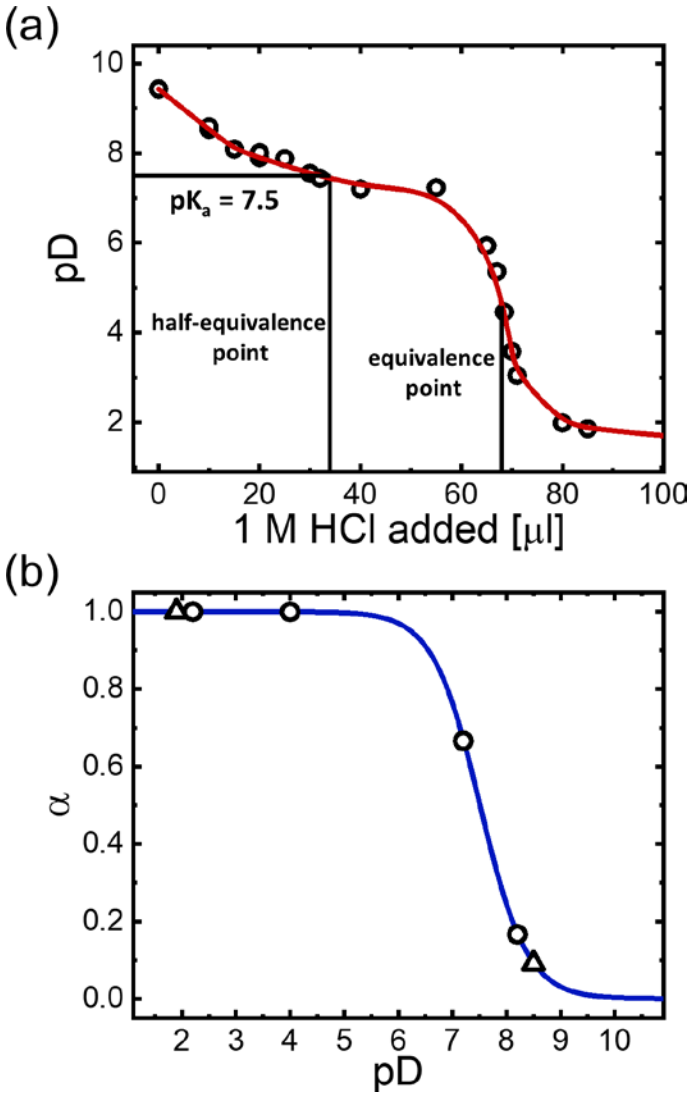

Figure 1. (a) Titration curve of a 1 wt% pentablock quaterpolymer solution in D_2O. The red line guides the eye. The equivalence point, the half-equivalence point and the resulting dissociation constant, pK_a, are indicated. (b) Calculated degree of ionization, α, of the PDMAEMA blocks as a function of the pD value. pD values of solutions used for SAXS/SLS/DLS and SANS experiments are indicated with open circles and open triangles, respectively.

pD and temperature dependence of the micellar size

DLS measurements were performed to determine the hydrodynamic radius of the micelles in dependence on the pD value in the range 2.2-8.2 and on temperature (10-60 °C). Data obtained from temperature-resolved DLS measurements at various pD values are compiled in Figure 2. At the pD values chosen (2.2, 4.0, 7.2 and 8.2), the degree of ionization of the PDMAEMA blocks is expected to be 1.00, 1.00, 0.67 and 0.17, respectively (Figure 1b). The autocorrelation functions shown in Figure 2a-d decay at times τ below ~1 ms. For all pD values, τ shifts to smaller values with increasing temperature. The shift is most pronounced at pD 8.2, which is an indication that it is not only due to the viscosity change of the solvent, but, especially at high pD values, may be related to the thermo-responsive behavior of PDMAEMA. A LCST of around 55 °C was previously found for linear $PDMAEMA_{108}$ at pH 8, which increases with decreasing degree of polymerization.[50] Therefore, for the $PDMAEMA_{50}$ blocks in the polymer under investigation here, we expect an LCST of at least 55 °C at pD > 8.

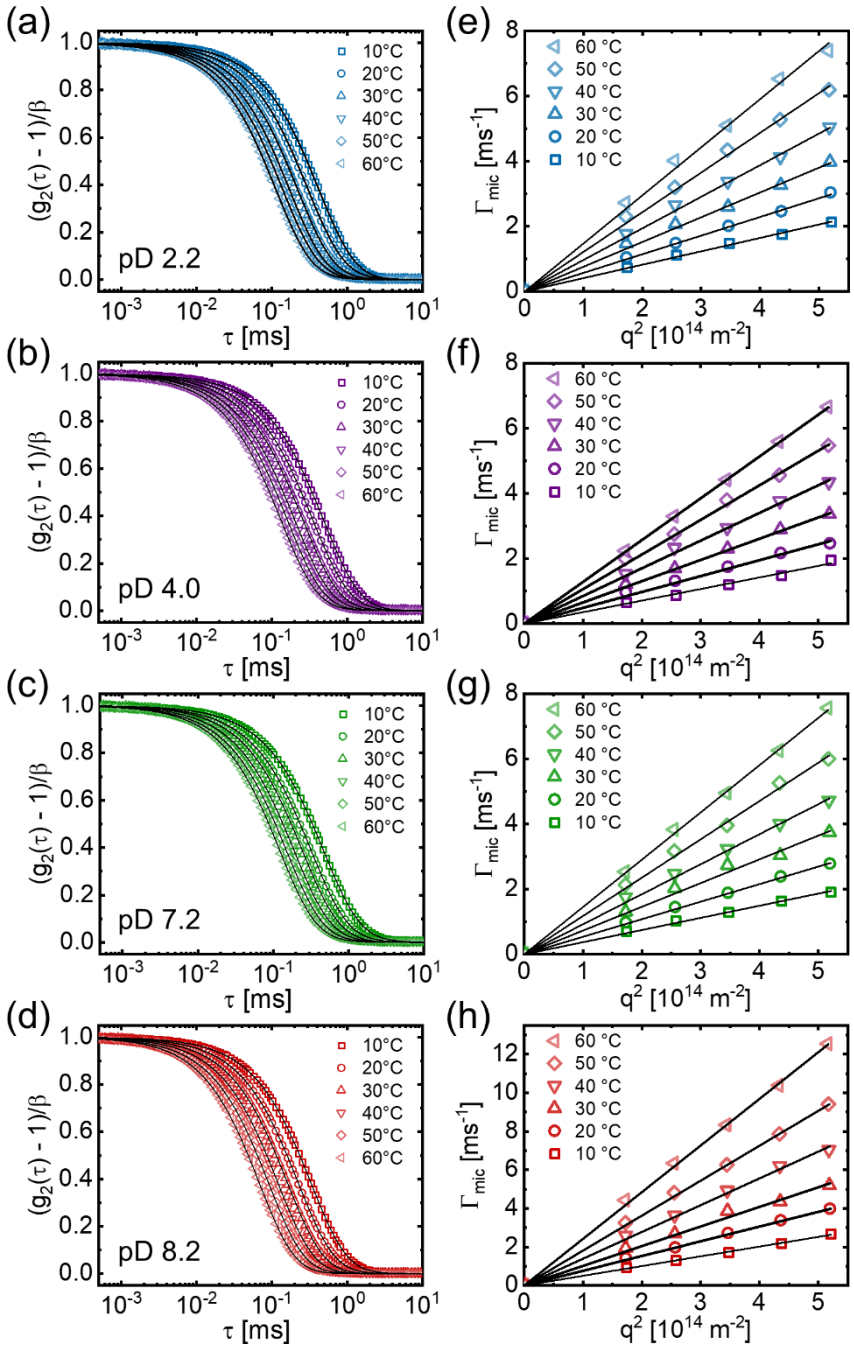

Figure 2. Results from DLS on 1 wt% solutions in D_2O measured at θ = 90° at the temperatures given in the graphs and at pD values of 2.2 (a, e,), pD 4.0 (b, f), pD 7.2 (c, g) and pD 8.2 (d, h). (a-d) Normalized autocorrelation functions (open symbols). Solid lines are model fits using eq 1. (e-h) Decay rates of the fast mode (open symbols), obtained from fitting $g_2(\tau)$-1 with eq 1, as a function of q^2. Solid lines are linear fits to the data.

A preliminary analysis of the autocorrelation functions by calculating the distribution functions of hydrodynamic radii, G(R_h) (see the Experimental Section) reveals rather broad peaks at pD 2.2, 4.0 and 7.2, which are centered at ~ 50 nm, independent of temperature (Figure S3 in the Supporting Information). In contrast, at pD 8.2, the distributions are narrower, are centered at ~20-30 nm, and shift slightly towards smaller sizes with increasing temperature.

It seems straightforward to attribute the particles to single micelles formed by the pentablock quaterpolymer with the P(*n*BuMA-*co*-TEGMA) end blocks forming the core, which is surrounded by a shell formed by the PDMAEMA-*b*-PEG-*b*-PDMAEMA part. While it is likely that such micelles are present in the solution, the peaks in the size distributions cannot be entirely due to single micelles for two reasons: (i) The contour length of the pentablock copolymer is calculated to be 49.7 nm (see the Supporting Information for details about the calculation). This value is the upper limit for the radius of a single micelle, but the size distributions extend to radii >100 nm. (Due to dispersity effects, higher contour length might be expected but are still estimated to be < 100 nm.) (ii) The size distributions are rather broad and skewed.

Therefore, it is reasonable to assume a bimodal distribution, i.e., in this case coexisting single micelles and larger clusters. Using values for the probability to reject below 0.01, it is indeed possible to fit the correlation functions with a size distribution containing both small (R_h ~ 25 nm) and large particles (R_h ~ 75 nm), as shown exemplarily in Figure S4 in the Supporting Information. Since the clusters are small (their R_h amounts only to ~3 times the one of the single micelles), it is important to use proper values for the probability to reject to prevent merging of the two peaks in the distributions and to distinguish micelles and clusters. For this reason, we refrain from further analyzing the correlation functions using a continuous size distribution, but instead use a sum of two decays (eq 1) to fit the autocorrelation functions. The model fits the data well (Figure 2a-d)

and gives values for the decay rates of single micelles (Γ_{mic}) and clusters (Γ_{clu}) as well as the relative amount of single micelles (A_{mic}). In Figure 2e-h, values obtained for Γ_{mic} are shown as a function of q^2. The linear dependence indicates diffusive behavior. The diffusion coefficient and, subsequently, the hydrodynamic radius of the micelles are calculated using the Stokes-Einstein equation (eq 2). Values for Γ_{clu} are shown in Figure S6 in the Supporting Information. They diverge slightly from linearity, which is attributed to a high dispersity of the clusters size. Nevertheless, we use the same procedure to estimate their average hydrodynamic radii.

The results are shown in Figure 3, both in dependence on temperature (Figure 3a,b) and on the pD value (Figure 3c,d). The hydrodynamic radius of the single micelles is found to be $R_h \cong$ 30-35 nm, independent of temperature for pD values of 2.2-7.2. In contrast, for pD 8.2, it is much lower, namely 25 nm at 10 °C and decreases further to 18 nm at 60 °C (Figure 3a). A similar behavior is observed for the clusters, where larger clusters with sizes between 80-130 nm are found at pD 2.2-7.2, but smaller ones with $R_h \cong$ 50-75 nm at pD 8.2. The larger R_h values of the micelles at higher degree of ionizations are in accordance with the stretching of the PDMAEMA blocks due to electrostatic repulsion, in agreement with previous observations on similar systems.[65,66] Interestingly, R_h is maximum at pD values of 4-7 (Figure 3c). A decrease of the micellar size at low pH values was previously observed for a telechelic triblock copolymer with a PDMAEMA midblock and was attributed to the screening effect of counter ions at the high ionic strength of the solution.[30]

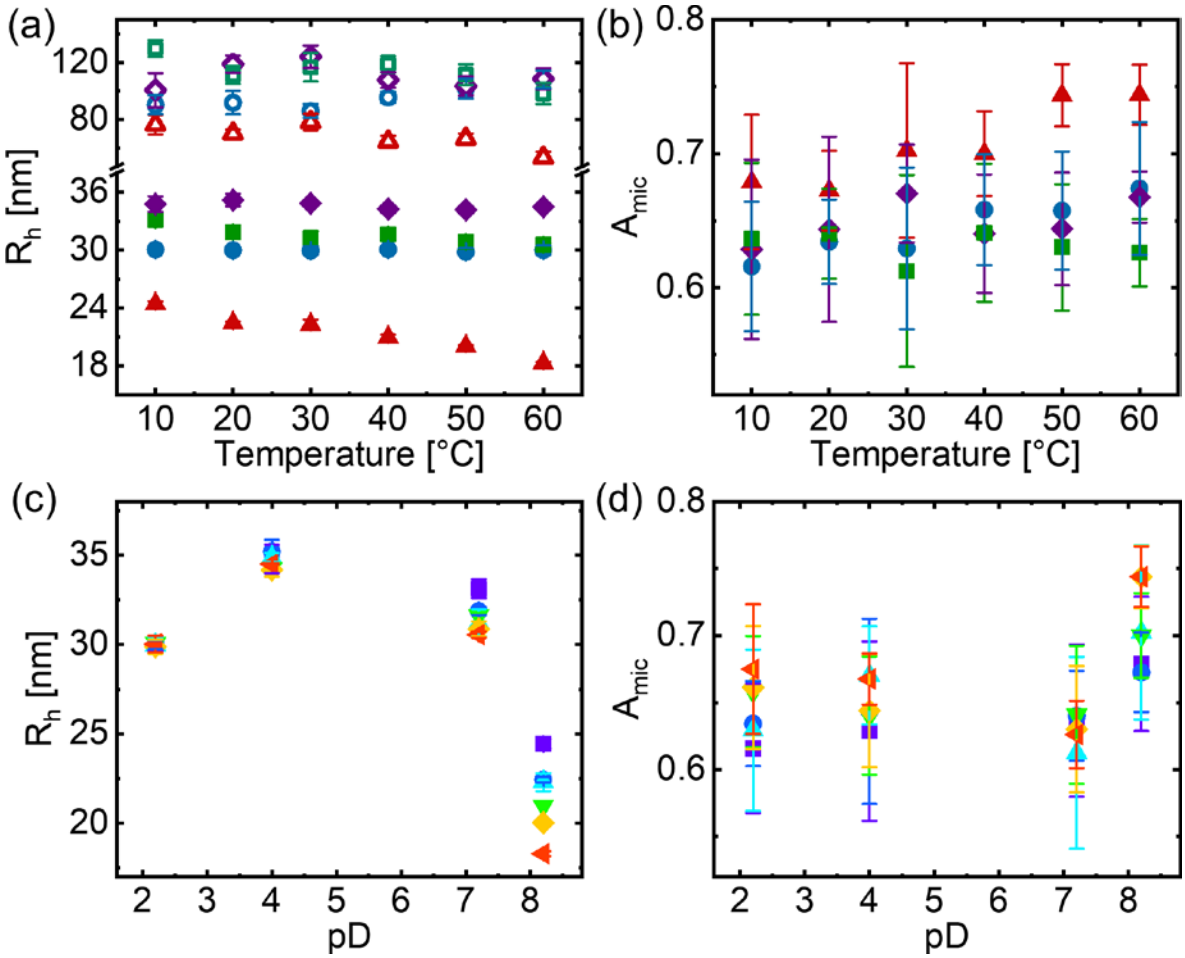

Figure 3. Results from fitting the DLS autocorrelation functions from Figure 2 using eq 1. (a) Hydrodynamic radii R_h of the micelles (filled symbols) and the clusters (open symbols) in dependence on temperature. Blue circles: pD 2.2, purple diamonds: pD 4.0, green squares: pD 7.2, red triangles: pD 8.2. (b) Amplitude of the fast mode A_{mic}, attributed to single micelles. The same data are shown in (c and d) in dependence on the pD value. Purple squares: 10 °C, blue circles: 20 °C, light blue triangles up: 30 °C, green triangles down: 40 °C, orange diamonds: 50 °C, red triangles left: 60 °C.

To characterize the size of the micelles, we estimate the upper limit for the radius of micelles with dangling ends or with loops (in each case, we assume the extreme case of fully stretched chains), which amount to 49.7 nm and 24.9 nm, respectively (Figure S5a,b in the Supporting

Information). We may further make the reasonable assumption that the very flexible PEG block assumes a random coil conformation. In this case, upper limits for dangling ends and loops amount to 36.8 nm and 20.2 nm, respectively (Figure S5c,d in the Supporting Information). More details about the calculation can be found in the Supporting Information. We note that, due to dispersity effects, higher values might be expected. For additional information regarding the size estimation of multiblock micelles, we refer to previous publications.[67,68]

At pD values of 2.2-7.2, R_h is significantly larger than the maximum radius of loops (even after separating off the contribution from the clusters), which might be attributed to a certain fraction of dangling ends. This means that the gain in enthalpy associated with incorporating hydrophobic end blocks into the micellar core is not large enough to outweigh the entropy loss associated with a loop conformation of the midblock.[13] This may be enhanced by the low hydrophobicity (low degree of polymerization and 50% hydrophilic comonomer content) of the dynamic sticky end blocks as well as by the high degree of ionization of the PDMAEMA blocks due to additional contributions from the electrostatic energy. The latter effect was previously identified in molecular dynamics simulations on telechelic triblock copolymers with a polyelectrolyte midblock,[31,69] and found in experimental work on telechelic triblock systems.[70,71] We note that the flexible PEG block may permit backfolding even at high degree of ionization.

At pD 8.2 and at 10 °C, the R_h values are in the range of the values for the maximum radius of loops. Since it is unlikely for the midblock to be fully stretched, considering the associated loss of entropy and the low degree of ionization, we attribute these high values to a certain fraction of dangling ends as well, which implies that the end blocks are not completely hydrophobic (far below the LCST of the TEGMA moieties).

The decrease of R_h with increasing temperature at pD 8.2 may be due to two effects: (i) the thermo-responsive behavior of PDMAEMA, i.e., collapse of PDMAEMA at high temperatures or (ii) backfolding of the PDMAEMA-*b*-PEG-*b*-PDMAEMA middle part into the same micellar core, resulting in loops. Backfolding is enabled by an increase of the hydrophobicity of the end blocks at high temperatures, thus increasing the enthalpic penalty of dangling ends. For none of the cases, a decrease of R_h with increasing temperature is observed at low pD values since (i) PDMAEMA does not have an LCST-type transition at those pD values, and (ii) the dangling ends are stabilized by a high degree of ionization of PDMAEMA, preventing backfolding of the midblocks.

The fraction of single micelles, A_{mic}, is shown in Figure 3b as a function of temperature. At pD 8.2, A_{mic} increases slightly with temperature, i.e., the fraction of clusters decreases. In contrast, at the lower pD values (2.2-7.2), A_{mic} remains constant with temperature. This indicates that, at pD 8.2, less bridges are formed between the micelles, i.e., fewer dangling ends are available. The decrease of R_h with increasing temperature mentioned above may therefore be explained by a transition of dangling ends to loops. Finally, A_{mic} is found to decrease with decreasing pD value (Figure 3d), as expected: the higher degree of ionization stabilizes dangling ends and increases their reach, which both favor the formation of clusters through bridging.

Inner micellar structures

Having demonstrated the existence of both single micelles and clusters in dilute solutions and the dependence of their hydrodynamic radius on pD and temperature, we performed small-angle neutron scattering experiments at low and high pD (high and low degree of ionization of PDMAEMA, respectively) to characterize the internal structure of the micelles. The experiments were performed on 2 wt% solutions at pD 1.9 and pD 8.5 at temperatures between 10 °C and 60 °C (Figure 4). Using D_2O as a solvent affords high scattering contrast. All curves have a similar

shape, which is characterized by a prominent shoulder at ~0.015 Å^{-1} and a second less pronounced shoulder at ~0.06 Å^{-1} (Figure 4a,b). These are tentatively assigned to the form factor scattering of (uncorrelated) single micelles. Additionally, at low q values (below 0.01 Å^{-1}), weak forward scattering is observed which is assigned to scattering from the larger clusters of micelles, including their inner structure.

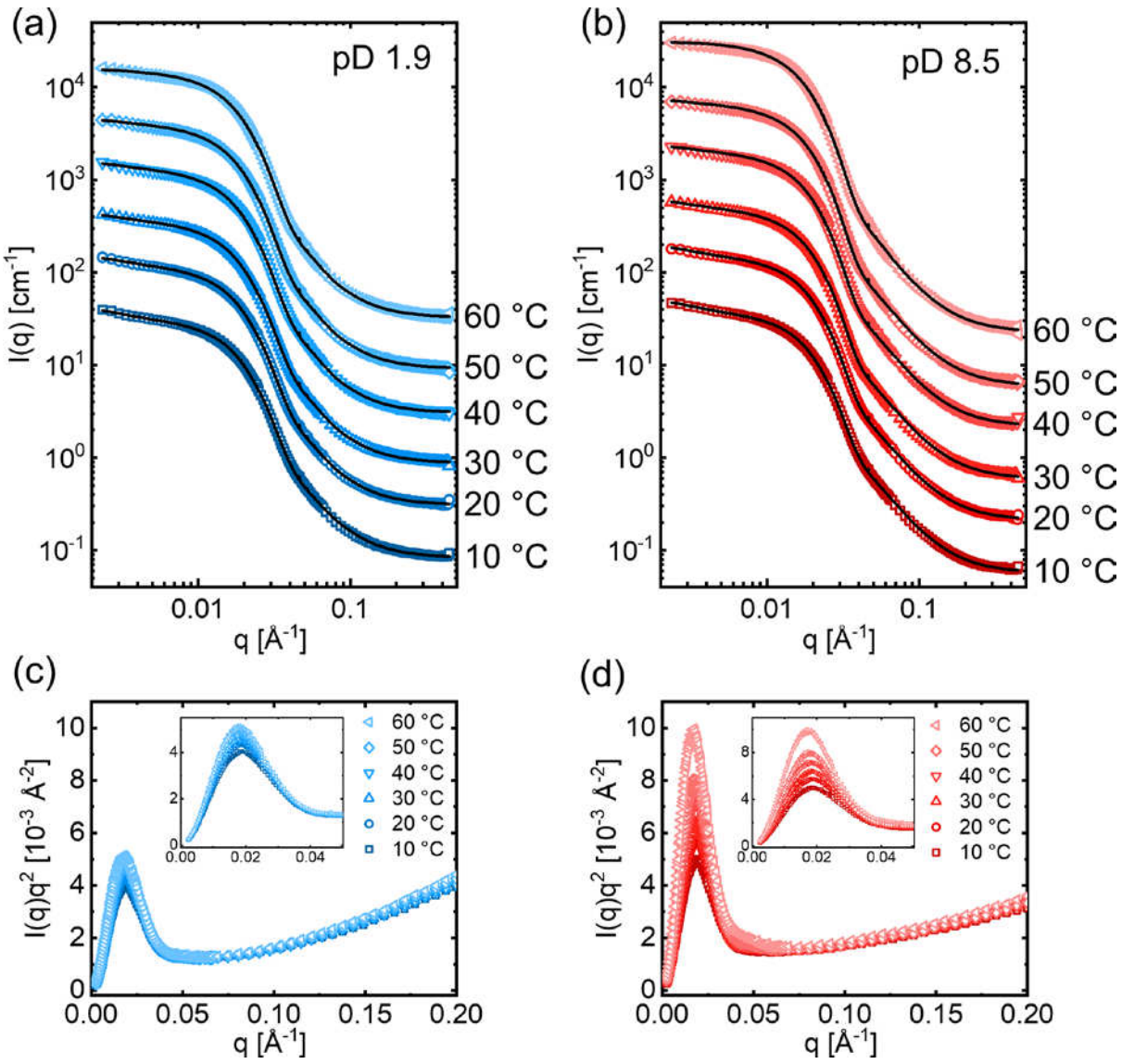

Figure 4. (a,b) SANS data of 2 wt% solutions at pD 1.9 (a) and pD 8.5 (b). Curves are shifted upwards by factors of 3.5, 10, 35, 100 and 350 for clarity. The data at 10 °C are therefore in

absolute units. From bottom to top: squares: 10 °C, circles: 20 °C, triangles up: 30 °C, triangles down: 40 °C, diamonds: 50 °C, triangle left: 60 °C. Black lines are best fits to the data (see text for details). (c,d) Kratky representation, $I(q)q^2$ vs q, of the same data at (c) pD 1.9 and (d) pD 8.5. The insets show a zoom of the low q part of the curve. Details of the incoherent background subtraction can be found in the Experimental Section.

More information is obtained from the Kratky representation of the scattering curves shown in Figure 4c,d. A peak at low q values indicates the presence of globular particles, which, in this case, are the more compact micellar cores presumably formed by the P(*n*BuMA-*co*-TEGMA) copolymer end blocks. For both pD values, the amplitude of the peak increases with temperature. At low temperatures, the copolymer end blocks may still be partially hydrophilic since the TEGMA units are water soluble. It is therefore reasonable to assume that the end blocks are partially hydrated, i.e., the core contains a certain amount of water, which we also found previously for micelles formed by triblock copolymers with very similar copolymer end blocks.[45] With increasing temperature, the TEGMA units become more hydrophobic, and water is expelled from the core, leading to a higher scattering contrast and increased scattering intensity. Towards higher q values, the curves in the Kratky plots first reach a plateau at intermediate q values, before they increase monotonically. This behavior is indicative of swollen chains and is attributed to the hydrophilic midblocks in the micellar shell.[72]

The shape of the SANS curves is significantly different from the ones observed by us previously on a 4 wt% solution of a P(nBuMA$_{18}$-*co*-TEGMA$_{15}$)-*b*-PDMAEMA$_{159}$-*b*-P(nBuMA$_{18}$-*co*-TEGMA$_{15}$) triblock terpolymer in D_2O at pH 6.6, which featured, among others, a pronounced maximum due to correlation of the micelles as well as strong forward scattering due to large clusters. A spherical core-shell form factor along with a hard-sphere structure factor and a Porod

form factor were used to model the curves.[45] The present curves neither feature a pronounced maximum nor strong forward scattering. Possible reasons may be the lower polymer concentration used here (2 wt%) and the shorter end blocks (overall 16 monomers compared to 33 previously). Another reason may be the presence of the PEG middle block which, due to its flexibility, may reduce the degree of bridging between the micelles and thus suppress the formation of large clusters. In combination with the shorter end blocks in the present quaterpolymer, this would lead to a larger fraction of dangling ends. Therefore, another model is used to describe the present data.[58]

We chose to analyze the present SANS data using a model describing uncorrelated micelles coexisting with clusters formed by the same type of micelles (eq 4).[58,59] The micelles are of spherical core-shell type, which have a homogenous core with a certain roughness. The shell has a radially decaying density profile and the scattering contribution of the shell blocks is given explicitly. Dangling ends as well as loops formed by the midparts are explicitly included. Models featuring a homogenous shell did not describe the data well. A certain number of micelles are randomly connected to form small clusters; these micelles are weakly correlated by a structure factor. This way, detailed information on the internal structure of the micelles can be obtained along with separate information on the clusters. Since the model contains numerous parameters, which may result in unstable fits, only a limited number of parameters are allowed to vary during fitting, namely the aggregation number of the micelles, N_{agg}, the micellar radius, R_m, the radius of gyration of the swollen chains in the shell, $R_{g,shell}$, the fraction of water in the core, f_{water}, and the fraction of clusters, f_{clu}. The core radius R_c is calculated from the volume of the end blocks, N_{agg} and f_{water} (eq 13). f_{loop} is found to have a minor effect on the outcome of the fit and is therefore fixed at a value of 0.5. SLD values of the shell and D_2O are fixed at the calculated values, see the

Exp. Section. The SLD of the core is a weighted average between its calculated value and the value of D_2O, based on f_{water}, in the fits. The relative width of the micellar surface, σ_m, and the roughness of the core-shell interface, σ_{int}, are found to give overall good fits at values of 0.1 and 10 Å, respectively, and are kept fixed. The parameter ν (interaction between chains in the shell) is fixed at -0.6 for pD 1.9 and -0.7 for pD 8.5. A negative value of ν is indicative of a repulsive interactions between polymer chains in the micellar shell, which are due to electrostatic repulsion of the positively charged PDMAEMA.[73] The fractal dimension describing the chain conformation in the shell, d_f, is found to describe the data best at a value of 2.3 and is kept fixed during fitting. N_{clu} and D were estimated from the R_h values of single micelles and clusters obtained from DLS and fixed at 30 and 50 nm, respectively. We note that a full fit to obtain the cluster size is not possible due to the limited q-range. Error-weighted residuals of the fits are shown in Figure S8a, which show that the model describes the data sufficiently well, considering that the system is complex (multi-segmented block copolymer). Systematic deviations are largely due to parameters that were kept fixed during fitting to prevent unstable fits, i.e., overfitting of the data.

The fit parameters are summarized in Figure 5. At pD 1.9, the micellar radius R_m (Figure 5a) increases from 13.7 nm at 10 °C to 13.9 nm at 60 °C. This behavior is in agreement with the one of R_h of the micelles in that only a small increase of R_m is observed. At pD 8.5, R_m increases from 12.6 nm to 14.1 nm, which is in contrast to the behavior of R_h, which decreases with increasing temperature. Moreover, the absolute values of R_m are significantly smaller than the ones of R_h, which cannot be explained only by the difference in concentration. Zinn et al. observed larger R_h values compared to R_m values in mixtures of diblock and telechelic block copolymers, and the deviation became larger with an increasing fraction of telechelic polymers.[58] Other studies on core-shell particles have attributed this deviation to the low density of chains in the outer part of the

shell, which do not contribute to the scattering, but influence the diffusion behavior of the micelle.[74–77] In our case, the difference between R_h and R_m corroborates the assumption made above that a certain fraction of end blocks are present as dangling ends, whereas SANS detects mainly the dense inner part of the shell. A sketch of the different radii measured with SANS and DLS is shown in Figure 6. Thus, a possible explanation for the temperature dependence of R_m at the high pD value is a transition from dangling ends to loops. The transition is promoted by the increase of hydrophobicity of the copolymer end blocks with temperature.

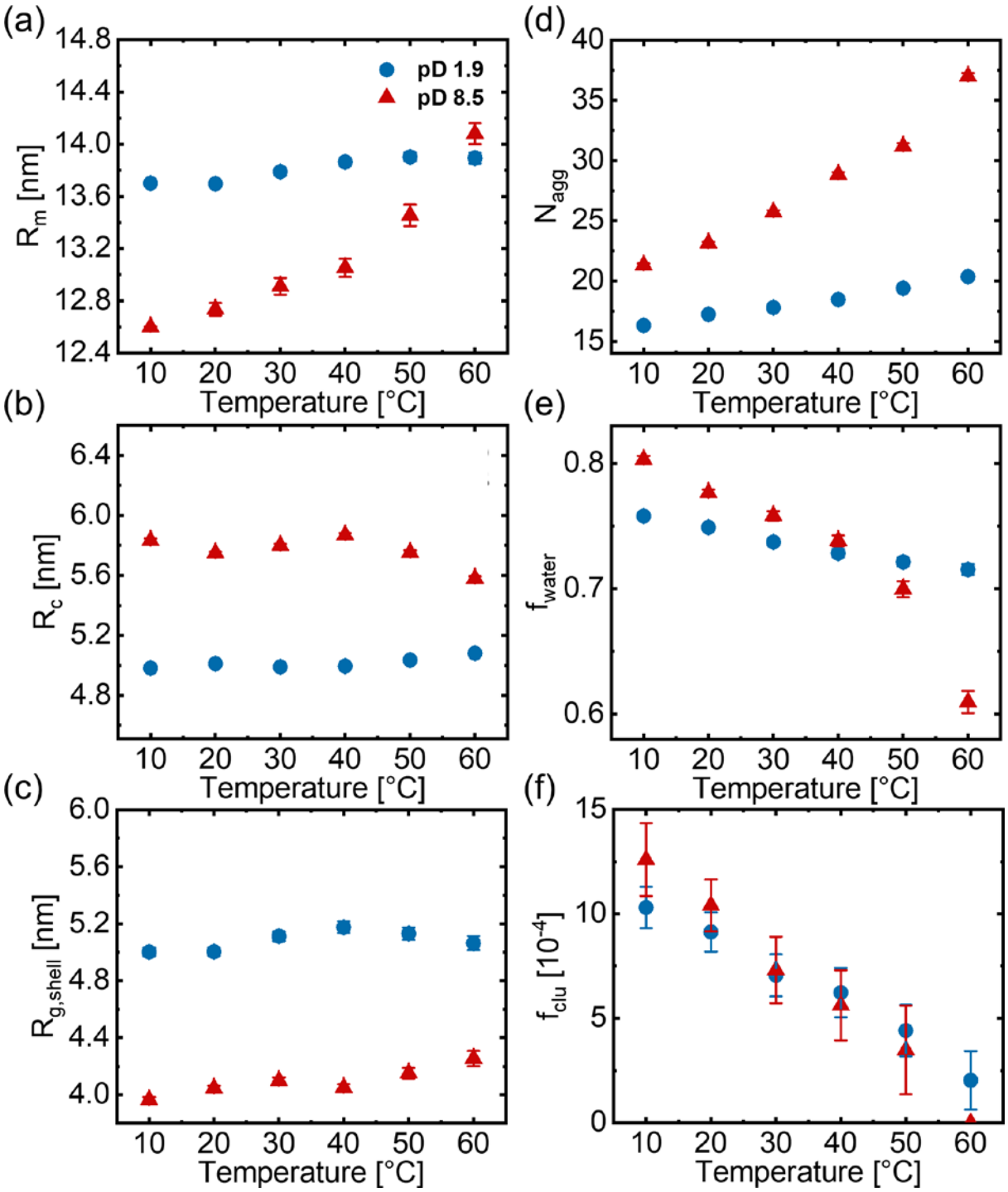

Figure 5. Temperature dependence of the parameters obtained from the model fits shown in Figure 4 at pD 1.9 (blue circles) and 8.5 (red triangles). (a) micellar radius R_m, (b) core radius R_c, (c) radius of gyration of polymer chains in the micellar shell, $R_{g,shell}$, (d) aggregation number N_{agg}, (e) fraction of water in the micellar core, f_{water}, (f) fraction of clusters, f_{clu}.

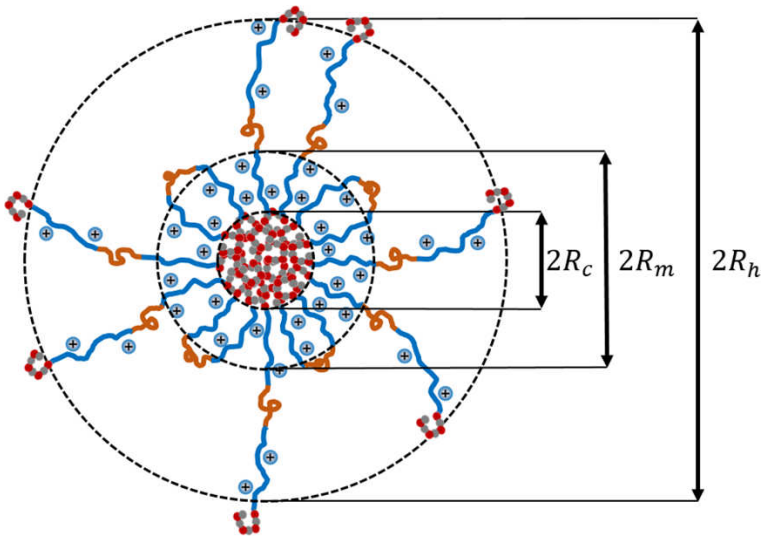

Figure 6. Schematic representation of a micelle formed by the telechelic pentablock quaterpolymer in a 2 wt% aqueous solution at pD values < pKa and at low temperatures. Colors represent TEGMA (red), *n*BuMA (grey), DMAEMA (blue) and EG (brown). The core and the micellar radius measured with SANS and the hydrodynamic radius measured with DLS are indicated and drawn to scale.

The core radius, R_c, is depicted in Figure 5b. It takes values between 4.9 nm and 5.1 nm at pD 1.9 and between 5.5 nm and 5.9 nm at pD 8.5 with no clear temperature dependence. The large core radius observed at pD 8.5 implies a dense arrangement of the PDMAEMA blocks attached to the core surface, which is most easily possible for the low charge density of the PDMAEMA blocks at this pD value.

The radius of gyration of the chains in the shell, $R_{g,shell}$, is shown in Figure 5c. At pD 1.9, $R_{g,shell}$ lies between 5.0 nm and 5.2 nm, and at pD 8.5 between 4.0 nm and 4.3 nm. The larger $R_{g,shell}$ at pD 1.9 compared to pD 8.5 may be attributed to the stretching of the PDMAEMA block due to its high degree of ionization (Figure 1b). The weak temperature dependence of $R_{g,shell}$ at both pD values implies that the PDMAEMA block does not undergo an LCST-type coil-to-globule transition up to 60 °C.

Figure 5d shows the aggregation number of the micelles, N_{agg}. At pD 1.9, N_{agg} increases from 16.3 to 20.4 and at pD 8.5 from 21.3 to 37.0. The smaller N_{agg} value at the higher degree of ionization agrees with previous results on diblock copolymer micelles with a charged shell, where electrostatic repulsion hinders aggregation at a high degree of ionization.[78] The significant increase of N_{agg} with increasing temperature at pD 8.5 may be related to a transition of dangling ends to loops. Since f_{loop} is fixed during fitting, an increased fraction of loops is indirectly reflected in the value of N_{agg}.

The fraction of water inside the micellar core, f_{water}, is shown in Figure 5e. At pD 1.9, it decreases from 0.76 to 0.72 and at pD 8.5 from 0.80 to 0.61. At both pD values, a significant amount of water is present in the micellar core, which confirms the assumption made above that the P(*n*BuMA-*co*-TEGMA) end blocks are hydrated. At higher temperatures, water is expelled from the core, which was also deduced from the Kratky plots (Figure 4c,d Altogether, the temperature-independent core radius can be explained by a balance between the volume uptake through the incorporation of additional end blocks (increase of N_{agg}) and the volume release through dehydration (water expulsion) from the micellar core. It is interesting to note that, even at 60 °C, a large amount of water is present in the micellar core, which may be attributed to the small size of the end blocks.

The relative amount of clusters, shown in Figure 5f, decreases with increasing temperature for both low and high pD values, but decreases more strongly at pD 8.5. This indicates that clusters are less likely to form, which might be due to the enhanced tendency of the micelles to form loops instead of dangling ends or bridges. We tentatively ascribe this tendency to an increased enthalpy of the end blocks at higher temperatures.

Verification of the structural model

The structural model used to describe the SANS data is rather complex and contains a relatively large number of fitting parameters, while the SANS data do not show a large amount of characteristic features. To verify whether the chosen model is appropriate and whether the parameters found are reasonable, we use data from SLS and SAXS experiments. These were performed on the identical solutions as in the DLS measurements. A comparison between SANS, SAXS and SLS scattering curves measured on similar solutions is shown in Figure 7a.

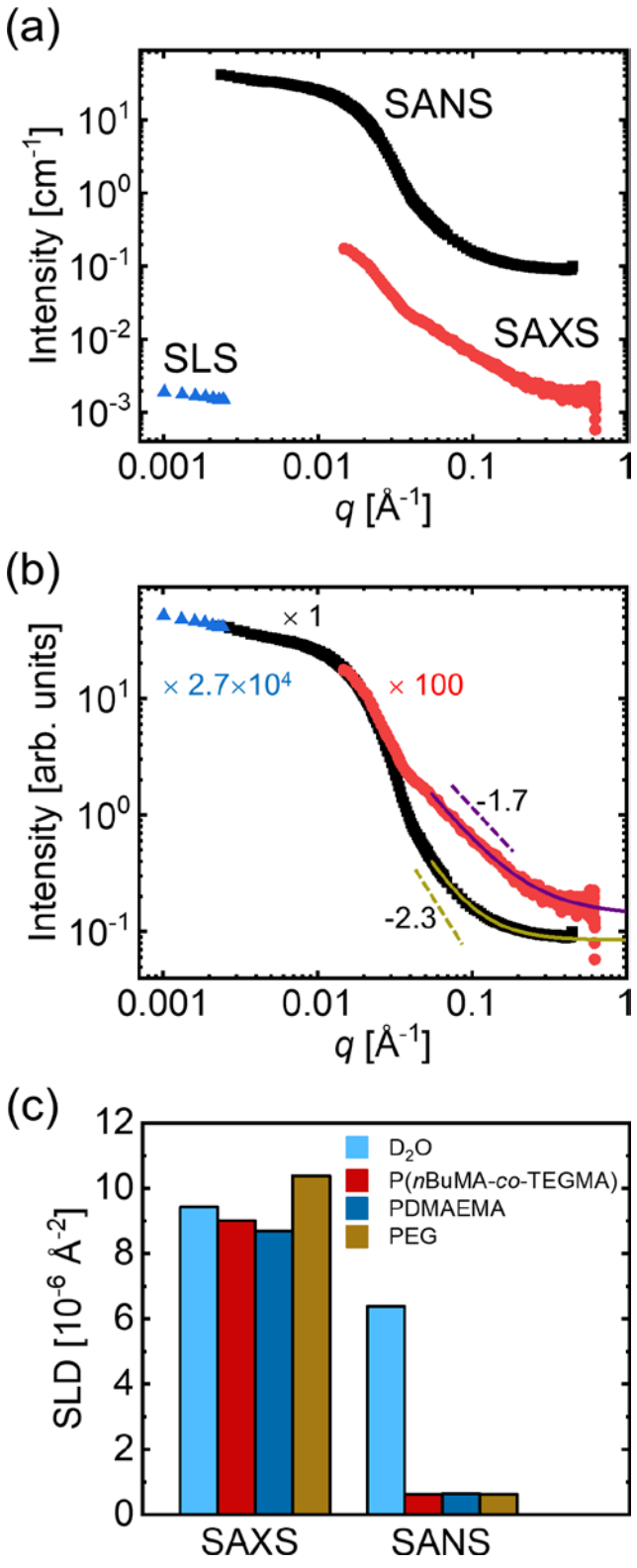

Figure 7. (a) Representative scattering curves measured with SANS (black squares), SAXS (red circles) and SLS (blue triangles) in absolute units. The SANS data are from a 2 wt% solution at

pD 1.9 and 20 °C and the SAXS/SLS data from a 1 wt% solution at pD 2.2 and 20 °C. (b) Same data as in (a), but with the SAXS and SLS curves shifted upwards by factors of 100 and 2.7×10^4, respectively. The slopes of the scattering curves in the high q region (> 0.05 Å^{-1}), which represent the exponent d_f of the single chain scattering contribution (eq 15), are indicated with dashed lines. Solid lines are the sum of a power law with exponent d_f and a constant background. (c) SLDs of D_2O, P(*n*BuMA-*co*-TEGMA), PDMAEMA and PEG for X-rays (λ = 1.54 Å) and neutrons (λ = 5 Å). The mass densities used for the calculation are given in the Exp. Section.

All data are measured on absolute scale, and the intensities of the SAXS and SLS data are approximately two and four orders of magnitude lower than the ones from SANS. The difference is partly due the difference in polymer concentration (1 wt% vs 2 wt%), but mainly to the different scattering contrast. It was shown that this difference can be accounted for by careful calculations of the respective scattering contrasts,[79] but this procedure relies on assumptions about the polymer-solvent interaction and is further complicated by the multiblock nature of the polymer in the present work. Another common procedure is to merge the curves by matching the intensities of overlapping parts of the scattering curves. For the SLS and SAXS data alone this is not feasible since there is a large gap between their respective q-ranges. We therefore use the SANS data as a qualitative extension of the SAXS data to allow merging of the SLS and SAXS data sets. Using suitable scaling factors, it is indeed possible to match the curves in the intermediate-q range (0.01-0.03 Å^{-1}) and in the low-q-range (< 0.003 Å^{-1}), as shown in Figure 7b.

A mismatch between the SAXS and SANS data in the high q-range is often observed[76,80] and may be due to contrast differences highlighting different parts of the micelle. (In our case, differences in the polymer concentration may contribute to the discrepancies as well.) In Figure 7c, the calculated SLDs of the different blocks and of D_2O are shown for both X-rays and neutrons.

The SLD of the P(*n*BuMA-*co*-TEGMA) random copolymer was calculated based on its composition and the SLDs of the respective monomers. While the scattering contrast between the polymer blocks and D_2O is larger in SANS, PEG has a significantly larger scattering contrast than the other blocks in SAXS. For this reason, we did not attempt to fit the combined SLS, SAXS curves and the SANS curves simultaneously, but instead fit the SLS and SAXS curves separately.

The combined SLS and SAXS scattering curves at 20 °C and all pD values are shown in Figure 8. Scattering curves at 30-60 °C can be found in Figure S7 in the SI. The slight slope in the SLS data confirms the existence of clusters, and therefore, the cluster structure factor (eq 5) is again included in the model fit. Due to the limited q-range of the SAXS data, the shoulder at low q (< 0.03 $Å^{-1}$), which is related to the micellar radius R_m, does not reach a plateau value. Since the absolute intensity of the plateau is mainly determined by N_{agg} and the scattering contrast, we fix f_{water} at a value of 0.75, which is estimated from the SANS results, to make the fits more reliable. As a result, R_c is not calculated from eq 13, but is treated as an independent fit parameter. A value of d_f = 1.7 is found to describe the data best and is fixed at this value. This value is smaller than the value used for SANS, which may be due to the lower concentration of the SAXS solution and the difference in contrast. ν is kept fixed during fitting at values of -0.85, -0.88, -0.90 and -0.92 for pD 2.2, pD 4.0, pD 7.2 and pD 8.2, respectively. All other parameters are chosen to match the ones used for the SANS analysis.

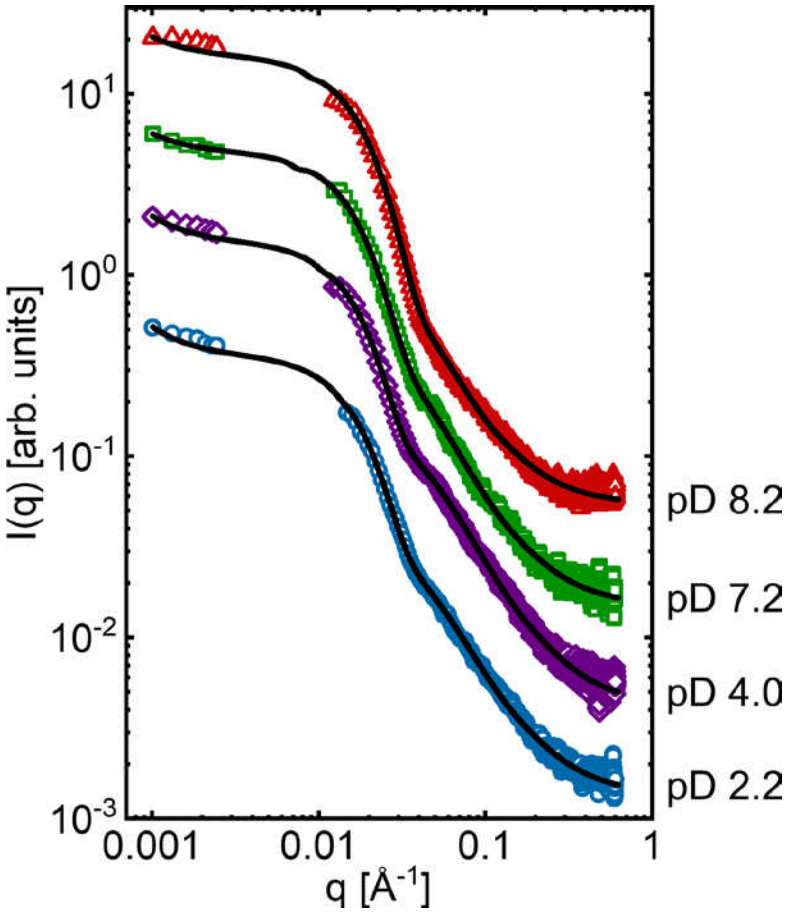

Figure 8. SLS (low q) and SAXS (high q) scattering curves of 1 wt% solutions at 20 °C and at pD 2.2 (blue circles), pD 4.0 (purple diamonds), pD 7.2 (green squares) and pD 8.2 (red triangles). Curves are shifted upwards by factors of 3.5, 10 and 35, respectively. The SAXS data at pD 2.2 are therefore in absolute units. Black lines are best fits to the data (see text for details).

The best model fits are indicated with solid lines in Figure 8 and in Figure S7 in the Supporting Information, respectively, and describe the data well. Error-weighted residuals of the fits are shown in Figure S8b. The fact that both, the SANS data and the combined SAXS and SLS data, can be fitted with the same model confirms its applicability to the investigated system. All relevant fit parameters of the model fits are summarized in Table S4 in the Supporting Information. Due to the low scattering contrast and limited q-range of the SAXS experiments, a detailed evaluation of

the fit parameters is difficult. Instead, we briefly highlight important qualitative agreements with the SANS results. The micellar radius R_m is maximum at low pD values and at high temperatures. R_m increases slightly with increasing temperature at all pD values. This is in full agreement with the SANS results. The overall values of R_m are in the range of the SANS results. The aggregation number N_{agg} is overall larger at high pD values compared to low pD values, which agrees with the SANS results. Due to the missing plateau value at the low-q end of the curve, we refrain from comparing the absolute values of N_{agg} found with SAXS to the ones found with SANS. Values of ν are negative and comparable to the SANS values. Values of R_c are on average in the range of the SANS values. A major difference between the SAXS and SANS parameters is the radius of gyration of single chains in the shell, $R_{g,shell}$. The SAXS values are on average significantly smaller than the SANS values and increase with increasing pD and with increasing temperature. For midblocks containing cationic polyelectrolytes, one would expect a decrease of $R_{g,shell}$ with decreasing degree of ionization (increasing pD),[31] which is also the result of the SANS analysis. We speculate that, due to this discrepancy and the fact that values of $R_{g,shell}$ are much smaller, SAXS mainly detects the PEG part of the midblock, because it has the highest scattering contrast for X-rays (Figure 7c). It is expected to behave as a single chain in a good solvent.

CONCLUSIONS

The structural properties of micelles formed by the multi-responsive telechelic pentablock quaterpolymer P(*n*BuMA$_8$-*co*-TEGMA$_8$)-*b*-PDMAEMA$_{50}$-*b*-PEG$_{46}$-*b*-PDMAEMA$_{50}$-*b*-P(*n*BuMA$_8$-*co*-TEGMA$_8$) in aqueous solution have been investigated as function of pD and temperature by DLS, SLS, SANS and SAXS. The polymer is similar to a previously investigated telechelic triblock terpolymer,[45] but has shorter end blocks and an additional central PEG block. Moreover, while the previous work focused on temperature-dependent rheological and structural properties at concentrations above the *cgc* and at constant pH, the present work addresses structural properties at concentrations below the *cgc*, i.e., where a 3D network is not formed, and on the effect of varying the pH (pD) value of the solution.

DLS and SANS studies gave detailed information on the size and inner structure of the micelles. The model used to fit the SANS data was verified by performing complementary SAXS and SLS experiments. Changing only the scattering length densities and a few fit parameters in a reasonable way, it was possible to describe both data sets well. Thus, it was confirmed that the model is appropriate for describing the given system. A summary of the results is schematically shown in Figure **9**.

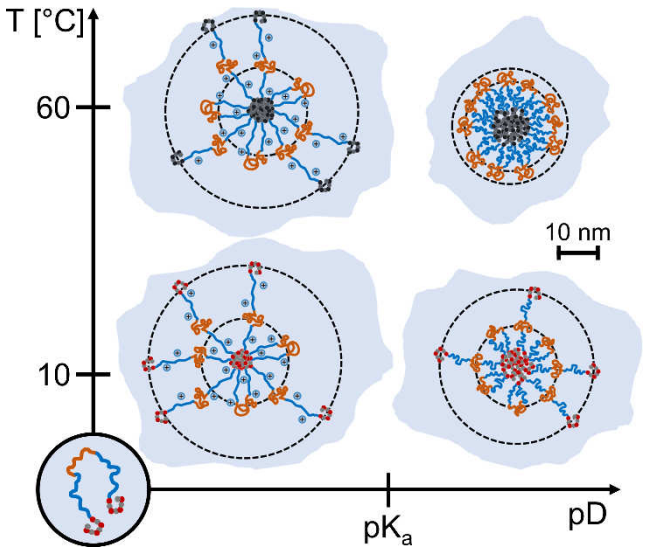

Figure 9. Schematic structures of the micelles formed by the pentablock quaterpolymer in aqueous solution at different pD and temperature conditions. Circles represent R_h (outer circle) and R_m (inner circle). All dimensions are drawn to scale. Colors represent TEGMA (red), *n*BuMA (grey), DMAEMA (blue) and EG (brown). The greyed out core at high temperatures indicates higher hydrophobicity. The scale bar gives a length scale.

At low temperatures, DLS data show coexistence of single micelles and small clusters at all pD values. The hydrodynamic radii of the micelles are generally larger at low pD values (< pK_a) compared to high pD values (> pK_a), which is due to stretching of the charged PDMAEMA blocks. It is also found that, at low pD values, more clusters form, which have a larger size compared to ones formed at high pD values. At least a fraction of the midblocks exist as dangling ends, which was deduced from estimating the maximum radius of a loop and comparing it to R_h. This is due to the short end blocks, which, at low temperatures, are still partially hydrophilic. SANS results confirm that a significant amount of water is present in the micellar cores. The aggregation number of the micelles and their core are found to be smaller at low pD values, due to high degree of

ionization of the PDMAEMA blocks that shift the hydrophobic/hydrophilic balance of the polymer to more hydrophilic.

The effect of increasing the temperature strongly depends on the pD value: At high pD values, dangling ends transition to loops, which is evidenced by a decrease of R_h found with DLS and increase of R_m found with SANS. This is due to the end blocks becoming more hydrophobic, which also results in larger aggregation numbers of the micelles and a lower fraction of water in the micellar core. As a result of fewer available dangling ends, less and smaller clusters are formed.

At low pD values, dangling ends are stable and no transition to loops is observed. As a result, R_h and R_m are only weakly dependent on temperature. An increase of the aggregation number of the micelles and decrease of the water fraction in the micellar core shows that, also at low pD values, the end blocks become hydrophobic. Therefore, the stabilization of the dangling ends is attributed to the high degree of ionization of the PDMAEMA blocks, which also enables cluster formation.

The results show that for telechelic polyelectrolytes with random copolymer end blocks, consisting of both hydrophobic and temperature-responsive monomers, decreasing the size of the end blocks and increasing the degree of ionization of the polyelectrolyte both favor the formation of dangling ends over loops. Furthermore, the temperature-dependence is not universal for all pD values but shows strong differences between low and high pD values. Regarding the ability to form a gel, we observed that replacing part of the polyelectrolyte midblock with a PEG block, while adding stealth properties and enhanced water solubility, increases the *cgc*. The results in this work indicate that the PEG block forms a random coil, i.e., it is not stretched, compared to a pure polyelectrolyte block, which, in the charged state, assumes a stretched conformation. A possible reason for the increased *cgc* is therefore the reduced effective length of the midblocks due to the

flexible PEG block. The increase of *cgc* might also be attributed to the enhanced tendency of the micelles to form loops instead of bridges due to the reduced entropic penalty of the midblock backfolding. Thus, more polymers are needed to cross the percolation threshold.

These insights into the self-assembly behavior of multisegmented multi-responsive polymers might be applied for improving the design of these kind of polymer systems for potential drug delivery application as micelles or hydrogels.

ASSOCIATED CONTENT

Supporting Information.

The Supporting Information is available free of charge on the ACS Publications website at DOI: xxx. Results from GPC and NMR. DLS size distributions. Calculation of contour length and estimation of the micellar size. DLS angular dependent decay rates of clusters. Additional SANS and SAXS data. (PDF)

AUTHOR INFORMATION

Corresponding Author

*E-mail papadakis@tum.de, phone +49 89 289 12 447, Fax +49 89 289 12 473 (C.M.P.).

Funding

We thank Deutsche Forschungsgemeinschaft (DFG) for financial support (PA 771/19-1).

Author Contributions

The manuscript was written through contributions of all authors. All authors have given approval to the final version of the manuscript.

Notes

The authors declare no competing financial interest.

ACKNOWLEDGMENT

We thank Reidar Lund from the University of Oslo for help with the model fits and fruitful discussions. This work is based upon experiments performed at the KWS-1 instrument operated by JCNS at the Heinz Maier-Leibnitz Zentrum (MLZ), Garching, Germany. We acknowledge beamtime allocation and excellent equipment.

REFERENCES

(1) Alexandridis, P. Amphiphilic Copolymers and Their Applications. *Curr. Opin. Colloid Interface Sci.* **1996**, *1*, 490–501.

(2) Hamley, I. W. *The Physics of Block Copolymers*; Oxford University Press: Oxford, 1999.

(3) Riess, G. Micellization of Block Copolymers. *Prog. Polym. Sci.* **2003**, *28*, 1107–1170.

(4) Gohy, J.-F. Block Copolymer Micelles. In *Block Copolymers II*; Abetz, V., Ed.; Springer Berlin Heidelberg: Berlin, Heidelberg, 2005; pp 65–136.

(5) Zhulina, E. B.; Borisov, O. V. Theory of Block Polymer Micelles: Recent Advances and Current Challenges. *Macromolecules* **2012**, *45*, 4429–4440.

(6) Raffa, P.; Wever, D. A. Z.; Picchioni, F.; Broekhuis, A. A. Polymeric Surfactants: Synthesis, Properties, and Links to Applications. *Chem. Rev.* **2015**, *115*, 8504–8563.

(7) Kwon, G. S.; Laird Forrest, M. Amphiphilic Block Copolymer Micelles for Nanoscale Drug Delivery. *Drug Dev. Res.* **2006**, *67*, 15–22.

(8) Cabral, H.; Miyata, K.; Osada, K.; Kataoka, K. Block Copolymer Micelles in Nanomedicine Applications. *Chem. Rev.* **2018**, *118*, 6844–6892.

(9) Bates, C. M.; Bates, F. S. 50th Anniversary Perspective: Block Polymers-Pure Potential. *Macromolecules* **2017**, *50*, 3–22.

(10) Balsara, N. P.; Tirrell, M.; Lodge, T. P. Micelle Formation of BAB Triblock Copolymers in Solvents That Preferentially Dissolve the A Block. *Macromolecules* **1991**, *24*, 1975–1986.

(11) Monzen, M.; Kawakatsu, T.; Doi, M.; Hasegawa, R. Micelle Formation in Triblock Copolymer Solutions. *Comput. Theor. Polym. Sci.* **2000**, *10*, 275–280.

(12) Pitto-Barry, A.; Barry, N. P. E. Pluronic® Block-Copolymers in Medicine: From Chemical and Biological Versatility to Rationalisation and Clinical Advances. *Polym. Chem.* **2014**, *5*, 3291–3297.

(13) Maiti, S.; Chatterji, P. R. Transition from Normal to Flowerlike Micelles. *J. Phys. Chem. B* **2000**, *104*, 10253–10257.

(14) Alami, E.; Almgren, M.; Brown, W.; François, J. Aggregation of Hydrophobically End-Capped Poly(ethylene oxide) in Aqueous Solutions. Fluorescence and Light-scattering Studies. *Macromolecules* **1996**, *29*, 2229–2243.

(15) Zhang, R.; Shi, T.; Li, H.; An, L. Effect of the Concentration on Sol-Gel Transition of Telechelic Polyelectrolytes. *J. Chem. Phys.* **2011**, *134*, 034903.

(16) Semenov, A. N.; Joanny, J. F.; Khokhlov, A. R. Associating Polymers: Equilibrium and Linear Viscoelasticity. *Macromolecules* **1995**, *28*, 1066–1075.

(17) Tuncaboylu, D. C.; Sari, M.; Oppermann, W.; Okay, O. Tough and Self-Healing Hydrogels Formed via Hydrophobic Interactions. *Macromolecules* **2011**, *44*, 4997–5005.

(18) Saunders, L.; Ma, P. X. Self-Healing Supramolecular Hydrogels for Tissue Engineering Applications. *Macromol. Biosci.* **2019**, *19*, 1800313.

(19) Tsitsilianis, C. Responsive Reversible Hydrogels from Associative "Smart" Macromolecules. *Soft Matter* **2010**, *6*, 2372–2388.

(20) Madsen, J.; Armes, S. P. (Meth)acrylic Stimulus-Responsive Block Copolymer Hydrogels. *Soft Matter* **2012**, *8*, 592–605.

(21) Sun, Y.; Liu, S.; Du, G.; Gao, G.; Fu, J. Multi-Responsive and Tough Hydrogels Based on Triblock Copolymer Micelles as Multi-Functional Macro-Crosslinkers. *Chem. Commun.* **2015**, *51*, 8512–8515.

(22) Lauber, L.; Santarelli, J.; Boyron, O.; Chassenieux, C.; Colombani, O.; Nicolai, T. pH- and Thermoresponsive Self-Assembly of Cationic Triblock Copolymers with Controlled Dynamics. *Macromolecules* **2017**, *50*, 416–423.

(23) Tsitsilianis, C.; Stavrouli, N.; Bocharova, V.; Angelopoulos, S.; Kiriy, A.; Katsampas, I.; Stamm, M. Stimuli Responsive Associative Polyampholytes based on ABCBA Pentablock Terpolymer Architecture. *Polymer* **2008**, *49*, 2996–3006.

(24) Determan, M. D.; Cox, J. P.; Seifert, S.; Thiyagarajan, P.; Mallapragada, S. K. Synthesis and Characterization of Temperature and pH-Responsive Pentablock Copolymers. *Polymer* **2005**, *46*, 6933–6946.

(25) Stavrouli, N.; Katsampas, I.; Aggelopoulos, S.; Tsitsilianis, C. pH/Thermosensitive

Hydrogels Formed at Low pH by a PMMA-PAA-P2VP-PAA-PMMA Pentablock Terpolymer. *Macromol. Rapid Commun.* **2008**, *29*, 130–135.

(26) Popescu, M. T.; Athanasoulias, I.; Tsitsilianis, C.; Hadjiantoniou, N. A.; Patrickios, C. S. Reversible Hydrogels from Amphiphilic Polyelectrolyte Model Multiblock Copolymers: The Importance of Macromolecular Topology. *Soft Matter* **2010**, *6*, 5417–5424.

(27) Chen, J.; Liu, M.; Gao, C.; Lü, S.; Zhang, X.; Liu, Z. Self-assembly Behaviors of pH- and Thermo-responsive Hydrophilic ABCBA-Type Pentablock Copolymers Synthesized by Consecutive RAFT Polymerization. *RSC Adv.* **2013**, *3*, 15085–15093.

(28) Radzevicius, P.; Steponaviciute, M.; Krivorotova, T.; Makuska, R. Double Thermoresponsive Pentablock Copolymers: Synthesis by One-Pot RAFT Polymerization and Self-Assembly in Aqueous Solutions. *Polym. Chem.* **2017**, *8*, 7217–7228.

(29) Salimi-Kenari, H.; Mirzadeh, H.; Nyström, B.; Dashtimoghadam, E.; Zhu, K.; Knudsen, K. D.; Forooqi Motlaq, V.; Hasani-Sadrabadi, M. M. Synthesis and Temperature-Induced Self-Assembly of a Positively Charged Symmetrical Pentablock Terpolymer in Aqueous Solutions. *Eur. Polym. J.* **2017**, *97*, 158–168.

(30) Bossard, F.; Aubry, T.; Gotzamanis, G.; Tsitsilianis, C. pH-Tunable Rheological Properties of a Telechelic Cationic Polyelectrolyte Reversible Hydrogel. *Soft Matter* **2006**, *2*, 510–516.

(31) Ghelichi, M.; Qazvini, N. T. Self-Organization of Hydrophobic-Capped Triblock Copolymers with a Polyelectrolyte Midblock: A Coarse-Grained Molecular Dynamics Simulation Study. *Soft Matter* **2016**, *12*, 4611–4620.

(32) Gotzamanis, G.; Papadimitriou, K.; Tsitsilianis, C. Design of a C-b-(A-co-B)-b-C Telechelic Polyampholyte pH-Responsive Gelator. *Polym. Chem.* **2016**, *7*, 2121–2129.

(33) Dyakonova, M. A.; Gotzamanis, G.; Niebuur, B. J.; Vishnevetskaya, N. S.; Raftopoulos, K. N.; Di, Z.; Filippov, S. K.; Tsitsilianis, C.; Papadakis, C. M. pH Responsiveness of Hydrogels Formed by Telechelic Polyampholytes. *Soft Matter* **2017**, *13*, 3568–3579.

(34) Zhao, C.; Ma, Z.; Zhu, X. X. Rational Design of Thermoresponsive Polymers in Aqueous Solutions: A Thermodynamics Map. *Prog. Polym. Sci.* **2019**, *90*, 269–291.

(35) Nykänen, A.; Nuopponen, M.; Laukkanen, A.; Hirvonen, S. P.; Rytelä, M.; Turunen, O.; Tenhu, H.; Mezzenga, R.; Ikkala, O.; Ruokolainen, J. Phase Behavior and Temperature-Responsive Molecular Filters Based on Self-Assembly of Polystyrene-*block*-Poly(*N*-isopropylacrylamide)-*block*-Polystyrene. *Macromolecules* **2007**, *40*, 5827–5834.

(36) Adelsberger, J.; Kulkami, A.; Jain, A.; Wang, W.; Bivigou-Koumba, A. M.; Busch, P.; Pipich, V.; Holderer, O.; Hellweg, T.; Laschewsky, A.; Müller-Buschbaum, P.; Papadakis, C. M. Thermoresponsive PS-*b*-PNIPAM-*b*-PS Micelles: Aggregation Behavior, Segmental Dynamics, and Thermal Response. *Macromolecules* **2010**, *43*, 2490–2501.

(37) Angelopoulos, S. A.; Tsitsilianis, C. Thermo-Reversible Hydrogels based on Poly(*N*,*N*-diethylacrylamide)-*block*-poly(acrylic acid)-*block*-poly(*N*,*N*-diethylacrylamide) Double Hydrophilic Triblock Copolymer. *Macromol. Chem. Phys.* **2006**, *207*, 2188–2194.

(38) Lin, Z.; Cao, S.; Chen, X.; Wu, W.; Li, J. Thermoresponsive Hydrogels from Phosphorylated ABA Triblock Copolymers: A Potential Scaffold for Bone Tissue Engineering. *Biomacromolecules* **2013**, *14*, 2206–2214.

(39) Despax, L.; Fitremann, J.; Destarac, M.; Harrisson, S. Low Concentration Thermoresponsive Hydrogels from Readily Accessible Triblock Copolymers. *Polym. Chem.* **2016**, *7*, 3375–3377.

(40) Tsitsilianis, C.; Gotzamanis, G.; Iatridi, Z. Design of "Smart" Segmented Polymers by Incorporating Random Copolymers as Building Blocks. *Eur. Polym. J.* **2011**, *47*, 497–510.

(41) Nicolai, T.; Colombani, O.; Chassenieux, C. Dynamic Polymeric Micelles Versus Frozen Nanoparticles Formed by Block Copolymers. *Soft Matter* **2010**, *6*, 3111–3118.

(42) Lejeune, E.; Drechsler, M.; Jestin, J.; Müller, A. H. E.; Chassenieux, C.; Colombani, O. Amphiphilic Diblock Copolymers with a Moderately Hydrophobic Block: Toward Dynamic Micelles. *Macromolecules* **2010**, *43*, 2667–2671.

(43) Charbonneau, C.; Chassenieux, C.; Colombani, O.; Nicolai, T. Controlling the Dynamics of Self-Assembled Triblock Copolymer Networks via the pH. *Macromolecules* **2011**, *44*, 4487–4495.

(44) Lauber, L.; Chassenieux, C.; Nicolai, T.; Colombani, O. Highlighting the Role of the Random Associating Block in the Self-Assembly of Amphiphilic Block-Random Copolymers. *Macromolecules* **2015**, *48*, 7613–7619.

(45) Tsitsilianis, C.; Serras, G.; Ko, C. H.; Jung, F.; Papadakis, C. M.; Rikkou-Kalourkoti, M.; Patrickios, C. S.; Schweins, R.; Chassenieux, C. Thermoresponsive Hydrogels Based on Telechelic Polyelectrolytes: From Dynamic to "Frozen" Networks. *Macromolecules* **2018**, *51*, 2169–2179.

(46) Zhang, J.; Farias-Mancilla, B.; Destarac, M.; Schubert, U. S.; Keddie, D. J.; Guerrero-

Sanchez, C.; Harrisson, S. Asymmetric Copolymers: Synthesis, Properties, and Applications of Gradient and Other Partially Segregated Copolymers. *Macromol. Rapid Commun.* **2018**, *39*, 1800357.

(47) Rabyk, M.; Destephen, A.; Lapp, A.; King, S.; Noirez, L.; Billon, L.; Hruby, M.; Borisov, O.; Stepanek, P.; Deniau, E. Interplay of Thermosensitivity and pH Sensitivity of Amphiphilic Block-Gradient Copolymers of Dimethylaminoethyl Acrylate and Styrene. *Macromolecules* **2018**, *51*, 5219–5233.

(48) Lutz, J. F. Polymerization of Oligo(Ethylene Glycol) (Meth)Acrylates: Toward New Generations of Smart Biocompatible Materials. *J. Polym. Sci. Part A Polym. Chem.* **2008**, *46*, 3459–3470.

(49) Plamper, F. A.; Synatschke, C. V; Majewski, A. P.; Schmalz, A.; Schmalz, H.; Müller, A. H. E. Star-shaped Poly[2-(dimethylamino)ethyl methacrylate] and its Derivatives: Toward New Properties and Applications. *POLIMERY* **2014**, *59*, 66–73.

(50) Plamper, F. A.; Ruppel, M.; Schmalz, A.; Borisov, O.; Ballauff, M.; Müller, A. H. E. Tuning the Thermoresponsive Properties of Weak Polyelectrolytes: Aqueous Solutions of Star-Shaped and Linear Poly(*N*,*N*-dimethylaminoethyl Methacrylate). *Macromolecules* **2007**, *40*, 8361–8366.

(51) Moad, G.; Chong, Y. K.; Postma, A.; Rizzardo, E.; Thang, S. H. Advances in RAFT Polymerization: The Synthesis of Polymers with Defined End-Groups. *Polymer* **2005**, *46*, 8458–8468.

(52) Glaseo, P. K.; Long, F. A. Use of Glass Electrodes to Measure Acidities in Deuterium

Oxide. *J. Phys. Chem.* **1960**, *64*, 188–190.

(53) Jakeš, J. Regularized Positive Exponential Sum (REPES) Program - A Way of Inverting Laplace Transform Data Obtained by Dynamic Light Scattering. *Collect. Czechoslov. Chem. Commun.* **1995**, *60*, 1781–1797.

(54) Štěpánek, P. Data Analysis in Dynamic Light Scattering. In *Dynamic Light Scattering: The Method and Some Applications (Monographs on the Physics and Chemistry of Materials)*; Brown, W., Ed.; Clarendon Press: New York, 1993; pp 177–241.

(55) Itakura, M.; Shimada, K.; Matsuyama, S.; Saito, T.; Kinugasa, S. A Convenient Method to Determine the Rayleigh Ratio with Uniform Polystyrene Oligomers. *J. Appl. Polym. Sci.* **2006**, *99*, 1953–1959.

(56) Heinz Maier-Leibnitz Zentrum; Frielinghaus, H.; Feoktystov, A. V.; Berts, I.; Mangiapia, G. KWS-1: Small-angle Scattering Diffractometer. *Journal of large-scale research facilities* **2015**, *1*, A28.

(57) Feoktystov, A. V.; Frielinghaus, H.; Di, Z.; Jaksch, S.; Pipich, V.; Appavou, M. S.; Babcock, E.; Hanslik, R.; Engels, R.; Kemmerling, G.; Kleines, H.; Ioffe, A.; Richter, D.; Brückel, T. KWS-1 High-resolution Small-angle Neutron Scattering Instrument at JCNS: Current State. *J. Appl. Crystallogr.* **2015**, *48*, 61–70.

(58) Zinn, T.; Willner, L.; Knudsen, K. D.; Lund, R. Self-Assembly of Mixtures of Telechelic and Monofunctional Amphiphilic Polymers in Water: From Clusters to Flowerlike Micelles. *Macromolecules* **2017**, *50*, 7321–7332.

(59) Zinn, T.; Willner, L.; Lund, R.; Pipich, V.; Appavou, M.-S.; Richter, D. Surfactant or Block

Copolymer Micelles? Structural Properties of a Series of Well-Defined *n*-alkyl–PEO Micelles in Water Studied by SANS. *Soft Matter* **2014**, *10*, 5212–5220.

(60) Schweins, R.; Huber, K. Particle Scattering Factor of Pearl Necklace Chains. *Macromol. Symp.* **2004**, *211*, 25–42.

(61) Monkenbusch, M.; Willner, L.; Allgaier, J.; Lindner, P.; Poppe, A.; Richter, D. Micellization of Amphiphilic Diblock Copolymers: Corona Shape and Mean-Field to Scaling Crossover. *Europhys. Lett.* **2000**, *51*, 628–634.

(62) Beaucage, G. Small-Angle Scattering from Polymeric Mass Fractals of Arbitrary Mass-Fractal Dimension. *J. Appl. Crystallogr.* **1996**, *29*, 134–146.

(63) Pedersen, J. S.; Posselt, D.; Mortensen, K. Analytical Treatment of the Resolution Function for Small-Angle Scattering. *J. Appl. Crystallogr.* **1990**, *23*, 321–333.

(64) Zhang, C.; Maric, M. Synthesis of Stimuli-responsive, Water-soluble Poly[2-(dimethylamino)ethyl methacrylate/styrene] Statistical Copolymers by Nitroxide Mediated Polymerization. *Polymers* **2011**, *3*, 1398–1422.

(65) Li, N. K.; Fuss, W. H.; Tang, L.; Gu, R.; Chilkoti, A.; Zauscher, S.; Yingling, Y. G. Prediction of Solvent-Induced Morphological Changes of Polyelectrolyte Diblock Copolymer Micelles. *Soft Matter* **2015**, *11*, 8236–8245.

(66) Betthausen, E.; Drechsler, M.; Förtsch, M.; Schacher, F. H.; Müller, A. H. E. Dual Stimuli-Responsive Multicompartment Micelles from Triblock Terpolymers with Tunable Hydrophilicity. *Soft Matter* **2011**, *7*, 8880–8891.

(67) Hadjiantoniou, N. A.; Triftaridou, A. I.; Kafouris, D.; Gradzielski, M.; Patrickios, C. S.

Synthesis and Characterization of Amphiphilic Multiblock Copolymers: Effect of the Number of Blocks on Micellization. *Macromolecules* **2009**, *42*, 5492–5498.

(68) Hadjiantoniou, N. A.; Krasia-Christoforou, T.; Loizou, E.; Porcar, L.; Patrickios, C. S. Alternating Amphiphilic Multiblock Copolymers: Controlled Synthesis via RAFT Polymerization and Aqueous Solution Characterization. *Macromolecules* **2010**, *43*, 2713–2720.

(69) Zhang, R.; Shi, T.; An, L.; Sun, Z.; Tong, Z. Conformational Study on Sol-Gel Transition in Telechelic Polyelectrolytes Solutions. *J. Phys. Chem. B* **2010**, *114*, 3449–3456.

(70) Gotzamanis, G. T.; Tsitsilianis, C.; Hadjiyannakou, S. C.; Patrickios, C. S.; Lupitskyy, R.; Minko, S. Cationic Telechelic Polyelectrolytes : Synthesis by Group Transfer Polymerization and Self-Organization in Aqueous Media Cationic Telechelic Polyelectrolytes : Synthesis by Group Transfer Polymerization and Self-Organization in Aqueous Media. *Macromolecules* **2006**, *39*, 678–683.

(71) Lemmers, M.; Spruijt, E.; Beun, L.; Fokkink, R.; Leermakers, F.; Portale, G.; Cohen Stuart, M. A.; van der Gucht, J. The Influence of Charge Ratio on Transient Networks of Polyelectrolyte Complex Micelles. *Soft Matter* **2011**, *8*, 104–117.

(72) Hsu, H. P.; Paul, W.; Binder, K. Scattering Function of Semiflexible Polymer Chains Under Good Solvent Conditions. *J. Chem. Phys.* **2012**, *137*, 174902.

(73) Sommer, C.; Pedersen, J. S. Temperature Dependence of the Structure and Interaction of Starlike PEG-Based Block Copolymer Micelles. *Macromolecules* **2004**, *37*, 1682–1685.

(74) Gohr, K.; Schärtl, W.; Willner, L.; Pyckhout-Hintzen, W. SANS Investigation of PS-PB

Block Copolymer Micelles in a Short Chain PB Homopolymer Matrix. *Macromolecules* **2002**, *35*, 9110–9116.

(75) Etampawala, T. N.; Aryal, D.; Osti, N. C.; He, L.; Heller, W. T.; Willis, C. L.; Grest, G. S.; Perahia, D. Association of a Multifunctional Ionic Block Copolymer in a Selective Solvent. *J. Chem. Phys.* **2016**, *145*, 184903.

(76) Sommer, C.; Pedersen, J. S.; Garamus, V. M. Structure and Interactions of Block Copolymer Micelles of Brij 700 Studied by Combining Small-Angle X-ray and Neutron Scattering. *Langmuir* **2005**, *21*, 2137–2149.

(77) Dulle, M.; Jaber, S.; Rosenfeldt, S.; Radulescu, A.; Förster, S.; Mulvaney, P.; Karg, M. Plasmonic Gold-poly(*N*-isopropylacrylamide) Core-Shell Colloids with Homogeneous Density Profiles: A Small Angle Scattering Study. *Phys. Chem. Chem. Phys.* **2015**, *17*, 1354–1367.

(78) Lee, A. S.; Bütün, V.; Vamvakaki, M.; Armes, S. P.; Pople, J. A.; Gast, A. P. Structure of pH-Dependent Block Copolymer Micelles: Charge and Ionic Strength Dependence. *Macromolecules* **2002**, *35*, 8540–8551.

(79) Jensen, G. V.; Shi, Q.; Hernansanz, M. J.; Oliveira, C. L. P.; Deen, G. R.; Almdal, K.; Pedersen, J. S. Structure of PEP-PEO Block Copolymer Micelles: Exploiting the Complementarity of Small-Angle X-ray Scattering and Static Light Scattering. *J. Appl. Crystallogr.* **2011**, *44*, 473–482.

(80) Pedersen, J. S. Analysis of Small-Angle Scattering Data from Colloids and Polymer Solutions: Modeling and Least-Squares Fitting. *Adv. Colloid Interface Sci.* **1997**, *70*, 171–

210.